

Calibration of the Tully-Fisher relation in the field

S. Rauzy

ANPE and Centre de Physique Théorique - C.N.R.S., Luminy Case 907, F-13288 Marseille Cedex 9, France.

Received / Accepted

Abstract. A new technique for calibrating slope and relative zero-point of Tully-Fisher like relations by using a sample of distant field galaxies is proposed. Based on a null-correlation approach (NCA), the technique is insensitive to the presence of selection effects on apparent magnitude m and on log line-width distance indicator p . This interesting property is used for discarding nearby galaxies of the observed sample. It is shown that such a subsampling allows in effect to attenuate biases on calibration parameters created by the presence of radial peculiar velocities.

Key words: galaxies – distance scale – velocity field

1. Introduction

During this last decade, increasing efforts have been made attempting to extract informations concerning the distribution of mass in the universe from the radial peculiar velocity field of distant galaxies (see for example Aaronson et al. 1986, Lynden-Bell et al. 1988, Bertschinger et al. 1990, Rauzy et al. 1992, Newsam et al. 1995, Rauzy et al. 1995). Quantitative results based on peculiar velocity studies, such as constraints on the value of the density parameter Ω_0 , can nowadays be found in the literature (see Dekel 1994 for a review). Reliability of such results is however closely related to the various working hypotheses assumed throughout the successive steps of the analysis.

First of these steps is to obtain redshift-independent estimates of galaxies distance. It is performed by using Tully-Fisher (TF) like relations (Tully-Fisher 1977 for spirals and Faber-Jackson 1976 for ellipticals). These observed statistical relations linearly correlate the absolute magnitude M (or similar quantity) of a galaxy with an observable parameter p ($p = \log V_{\text{rot}}$ for spirals and $p = \log \sigma$ for ellipticals). Assuming that the TF relation has been

correctly calibrated, an estimate of the absolute magnitude M is obtained by measuring the observable p . Measurement of the apparent magnitude m (or similar quantity) provides then with an estimate of the distance of the galaxy, and comparing it with the redshift z finally furnishes the deviation from the mean Hubble flow (i.e. the radial peculiar velocity).

The preliminar calibration step of the TF relation is of crucial importance for kinematical analyses since errors on the calibration parameters interpret indeed as fictitious large-scale and coherent peculiar velocity fields. Unfortunately, selection effects in observation, such as upper bound in apparent magnitude, bias the estimates of the TF calibration parameters. Many studies devoted to correct on these biases have been already proposed (see for example Schechter 1980, Bottinelli et al. 1986, Lynden-Bell et al. 1988, Fouqué et al. 1990, Hendry&Simmons 1990, Teerikorpi 1990, Bicknell 1992, Triay et al. 1994, Willick 1994, Hendry&Simmons 1994, Sandage 1994, Willick et al. 1995, Willick et al. 1996, Rauzy&Triay 1996, Ekhholm 1996, Triay et al. 1996).

Motivations leading to introduce a new calibration technique are twofold. First, bias correction requires generally a full description of the calibration sample (i.e. the specific shapes of the observational selection function on m and p and of the luminosity function have to be assumed). Since available samples are often constituted of data inherited from various observational programs, modelization of such characteristics still remains a difficult problem. The philosophy is herein to reduce as far as possible the number of dubious assumptions made on these composite samples when deriving calibration parameters. Second, it is not clear how existing calibration procedures are affected by the presence of radial peculiar velocities. The aim is herein to quantify, and if possible to minimize, influences of peculiar velocity fields on the estimates of the calibration parameters.

In section 2 is summarized the basic statistical model describing Tully-Fisher like relations. The new calibration technique is presented section 3. Cumbersome calculations and proofs can be found appendices A, B and C. Potentialities of the method are illustrated appendix D where

Send offprint requests to: S. Rauzy (rauzy@cpt.univ-mrs.fr)

NCA calibration of the Mathewson spirals field galaxies sample is performed.

2. Distance and velocity estimates

The Tully-Fisher like relations are based on an observed linear correlation between the absolute magnitude M (or similar quantity such as $-5 \log_{10} D$ with D the linear diameter) and the log line-width distance indicator p of galaxies ($p \approx \log V_{\text{rot}}$ for spirals and $p \approx \log \sigma$ for ellipticals). They allow to estimate distance and radial peculiar velocity of an individual galaxy from its measured apparent magnitude m (or similar quantity such as $-5 \log_{10} d$ with d the apparent diameter), parameter p and redshift z . In this section, we recall in mind the basic statistical model describing these relations (see Triay et al. 1994 or Rauzy & Triay 1996 for details).

Regardless of the distance of the galaxy, selection effects in observation and measurement errors, the theoretical probability density (pd) in the M - p plane reads :

$$dP_1 = F(M, p) dM dp \quad (1)$$

The Direct (i.e. Forward) Tully-Fisher (DTF) relation assumes that it exists a random variable ζ^D ,

$$\zeta^D = \widetilde{M}(p) - M = a^D p + b^D - M \quad (2)$$

statistically independent on p such as the theoretical pd of Eq. (1) rewrites :

$$dP_1 = f_p(p) dp g(\zeta^D; 0, \sigma_{\zeta}^D) d\zeta^D \quad (3)$$

where $f_p(p)$ is the distribution function of the variable p in the M - p plane. The random variable ζ^D of zero mean and dispersion σ_{ζ}^D accounts for the intrinsic scatter about the DTF straight line Δ_{DTF} of zero-point b^D and slope a^D . The distance modulus μ of an object reads :

$$\mu = m - M = 5 \log_{10} r + 25 \quad (4)$$

where m is the apparent magnitude of the galaxy and r its distance in Mpc. Regardless of measurement errors, the observed probability density takes the following form :

$$dP_2 = \frac{1}{A_2} \phi(m, p) f_p(p) dp g(\zeta^D; 0, \sigma_{\zeta}^D) d\zeta^D h(\mu) d\mu \quad (5)$$

where $\phi(m, p)$ is a selection function accounting for selection effects in observation on m and p , $h(\mu)$ is the spatial distribution function of sources (along the line-of-sight) and $A_2 = \int \phi(m, p) f_p(p) g(\zeta^D; 0, \sigma_{\zeta}^D) h(\mu) dp d\mu d\zeta^D$ is the normalisation factor warranting $\int dP_2 = 1$. Under the three following assumptions :

– $\mathcal{H}0$) No measurement errors on m and p are present.

Particularly, corrections on galactic extinction and on inclination effects are supposed valid.

– $\mathcal{H}1$) The function $g(\zeta^D; 0, \sigma_{\zeta}^D)$ is gaussian.

– $\mathcal{H}2$) Galaxies are homogeneously distributed in space, which implies that, whatever the line-of-sight direction, the distance modulus distribution function reads $h(\mu) = \exp[3\alpha\mu]$ with $\alpha = \frac{\ln 10}{5}$.

a statistical estimator \tilde{r} generally adopted for the distance of a galaxy with measured m and p reads as follows (see appendix A for details, or Lynden-Bell et al. 1988 Landy & Szalay 1992, Triay et al. 1994) :

$$\tilde{r} = \exp[\alpha(m - a^D p - b^D - 25)] \exp[\frac{7}{2}\alpha^2 \sigma_{\zeta}^D] \quad (6)$$

where the term $\exp[\frac{7}{2}\alpha^2 \sigma_{\zeta}^D]$ accounts for a volume correction. This unbiased¹ distance estimator does not depend on the selection function $\phi(m, p)$ in m and p and on the specific shape of the distribution function $f_p(p)$. Its accuracy $\Delta\tilde{r}$ is proportional to the distance estimate of the galaxy (see appendix A) :

$$\Delta\tilde{r} = \tilde{r} \sqrt{\exp[\alpha^2 \sigma_{\zeta}^D] - 1} \quad (7)$$

The radial peculiar velocity v of a galaxy, expressed in km s^{-1} with respect to the velocity frame in which the redshift z is measured, reads :

$$v = z - H_0 r \quad (8)$$

where H_0 is the Hubble's constant and z is expressed in km s^{-1} units. Assuming that the above hypotheses hold, the estimator \tilde{v} of the radial peculiar velocity of a galaxy with measured m , p and z reads thus as follows :

$$\tilde{v} = z - H_0 \tilde{r} = z - B \exp[\alpha(m - a^D p)] \exp[\frac{7}{2}\alpha^2 \sigma_{\zeta}^D] \quad (9)$$

where H_0 and b^D have been merged into a single parameter $B = H_0 \exp[\alpha(-b^D - 25)]$. The accuracy $\Delta\tilde{v}$ of this radial peculiar velocity estimator \tilde{v} is :

$$\Delta\tilde{v} = H_0 \Delta\tilde{r} = H_0 \tilde{r} \sqrt{\exp[\alpha^2 \sigma_{\zeta}^D] - 1} \quad (10)$$

3. Calibration using null-correlation approach

Presence of the radial peculiar velocities v are included in the statistical modelization by rewriting the density probability dP_2 of Eq. (5) as follows :

$$dP_3 = \frac{1}{A_3} \phi(m, p) f_p(p) dp g(\zeta^D) d\zeta^D h(\mu) d\mu f_v(v; \mathbf{x}) dv \quad (11)$$

¹ The estimator \tilde{r} given Eq. (6) is unbiased in the following sense. Suppose a sample of N galaxies homogeneously distributed in space and with the same measured m and p . For N large enough, the distances average on the sample $\langle r \rangle$ will coincide with the estimator \tilde{r} (i.e. $\langle r \rangle \rightarrow E(r | m, p) = \tilde{r}$ where $E(r | m, p)$ is the mathematical expectancy of r , given m and p). The statistics of Eq. (6) is generally used for inferring the distance of individual galaxies. It amounts to apply the above statistical formalism on a sample containing only one object, which cannot be done without ambiguousness.

where $f_v(v; \mathbf{x})$ is the distribution function of radial peculiar velocities depending in general on the spatial position $\mathbf{x} = (r \cos l \cos b, r \sin l \cos b, r \sin b)$ with (l, b) the direction of the line-of-sight in galactic coordinates.

The aim is herein to estimate the calibration parameters of the DTF relation entering into the radial peculiar velocity estimator \tilde{v} of Eq (9) (i.e. the DTF slope a^D and DTF "zero-point" defined as $B^* = B \exp[\frac{7}{2}\alpha^2 \sigma_\zeta^D]$). The calibration sample is constituted of field galaxies selected along the same line-of-sight of direction (l, b) for which apparent magnitude m , log line-width distance indicator p and redshift z are measured. It is assumed hereafter that the sample is described by the density probability of Eq. (11) and satisfies the following hypotheses :

- $\mathcal{H}0$) After appropriate corrections (galactic extinction, inclination effects, ...), residual measurement errors can be neglected.
- $\mathcal{H}1$) $g(\zeta^D)$ is gaussian, i.e. $g(\zeta^D) = g_G(\zeta^D; 0, \sigma_\zeta^D)$.
- $\mathcal{H}2$) The distance modulus distribution function reads $h(\mu) = \exp[3\alpha\mu]$ with $\alpha = \frac{\ln 10}{5}$.
- $\mathcal{H}3$) The distribution of radial peculiar velocities v is a gaussian of mean u and dispersion σ_v , i.e. $f_v(v; \mathbf{x}) = g_G(v; u, \sigma_v)$.

Since the calibration sample is constituted of galaxies lying in the field, $\mathcal{H}2$ appears as a reasonable assumption. Anyway, if the line-of-sight direction of the sample goes across a physical cluster, nothing prevents us to discard galaxies known to belong to the cluster.

Assumption $\mathcal{H}3$ implies that the radial peculiar velocity field is not correlated with the distance r . $\mathcal{H}3$ is thus ruled out if flows such like the Great Attractor are present along the line-of-sight. On the other hand, $\mathcal{H}3$ is less restrictive than the pure Hubble's flow hypothesis (i.e. $v = 0$ everywhere). First, galaxies may have a Maxwellian agitation of velocity dispersion σ_v . Second, the mean radial peculiar velocity along the line-of-sight u is not forced to zero. It allows to mimic the following situation. Suppose that a whole-sky sample is calibrated in a velocity frame of reference where sampled galaxies are not globally at rest (say that the sample has a bulk flow $\mathbf{u} = (u_x, u_y, u_z)$ in cartesian galactic coordinates with respect to the velocity frame of reference). The radial peculiar velocity of galaxies belonging to the same line-of-sight of direction (l, b) will be shifted by $u = u_x \cos l \cos b + u_y \sin l \cos b + u_z \sin b$. Assumption $\mathcal{H}3$ in fact tolerates this kind of situation.

3.1. NCA calibration of the DTF slope a^D

Calibration of the DTF slope a^D using null-correlation approach (NCA) is based on the following remark. For a calibration sample satisfying assumptions $\mathcal{H}0, \mathcal{H}1, \mathcal{H}2$ and $\mathcal{H}3$ with $u = \sigma_v = 0$ (i.e. pure Hubble's flow hypothesis), the variable $X = X(a^D)$ defined as :

$$X = X(a^D) = \alpha(m - a^D p) - \ln z \quad (12)$$

is not correlated with p (see appendix C for proof) :

$$\text{If } u = \sigma_v = 0 \text{ then } \text{Cov}(p, X(a^D)) = 0 \quad (13)$$

where $\text{Cov}(p, X) = E(pX) - E(p)E(X)$ is the covariance of variables p and X . On the other hand, a wrong value of the DTF slope (i.e. $a_F = a^D + \Delta a$) correlates p and the random variable $X(a_F) = \alpha(m - a_F p) - \ln z$:

$$\text{Cov}(p, X(a_F)) = \Delta C_0 = -\alpha \Delta a \text{Cov}(p, p) \neq 0 \quad (14)$$

where $\text{Cov}(p, p) = E([p - E(p)]^2) = \Sigma(p)^2$ is the square of the standard deviation of p . The null-correlation approach consists in to adopt the value of the parameter a verifying $\text{Cov}(p, X(a)) = 0$ as the correct estimate of the DTF slope a^D :

$$\text{NCA estimate of } a^D : a \text{ such } \text{Cov}(p, X(a)) = 0 \quad (15)$$

which gives in practice :

$$a^{\text{NCA}} = \frac{\text{Cov}(p, m)}{\text{Cov}(p, p)} - \frac{1}{\alpha} \frac{\text{Cov}(p, \ln z)}{\text{Cov}(p, p)} \quad (16)$$

Note that in the case of pure Hubble's flow, the NCA is a quite robust technique for calibrating the slope of the DTF relation. It furnishes indeed an unbiased estimate of a^D whatever the selection effects $\phi(m, p)$ on m and p which affect the observed sample, and whatever the specific shape of the theoretical distribution function $f_p(p)$ of the variable p (see appendix C).

Unfortunatly, the presence of radial peculiar velocities such as the ones assumed in $\mathcal{H}3$ with $u \neq 0$ or $\sigma_v \neq 0$ biases the NCA estimate of the slope a^D since Eq. (13) rewrites in this case (see appendix C) :

$$\text{Cov}(p, X(a^D)) = -\text{Cov}(p, \ln[1 + \frac{v}{H_0 r}]) \neq 0 \quad (17)$$

However, the magnitude of this bias can be attenuated by selecting only distant galaxies of the observed sample. It is not surprising since the term $\ln[1 + v/(H_0 r)]$ in Eq. (17) becomes negligible for distances r large enough. Such a subsampling can be performed by discarding galaxies of the observed sample which have a distance estimate \tilde{r} smaller than a given r^* . It corresponds to introduce an extra selection function $\psi(m, p)$ defined as follows :

$$\psi(m, p) = 1 \text{ if } \tilde{r} \geq r^* ; \psi(m, p) = 0 \text{ otherwise.} \quad (18)$$

where \tilde{r} is given Eq. (6). Introducing this extra selection effect does not alterate the result obtained Eq. (13) since this property is insensitive to the specific shape adopted for the selection function on m and p .

In order to evaluate amplitude of the bias appearing Eq. (17) and its variation with respect to the cut-off in distance estimate r^* , calculations have been performed on a synthetic sample characterized as follows :

- $\mathcal{H}0, \mathcal{H}1, \mathcal{H}2$ and $\mathcal{H}3$ are satisfied by the sample.

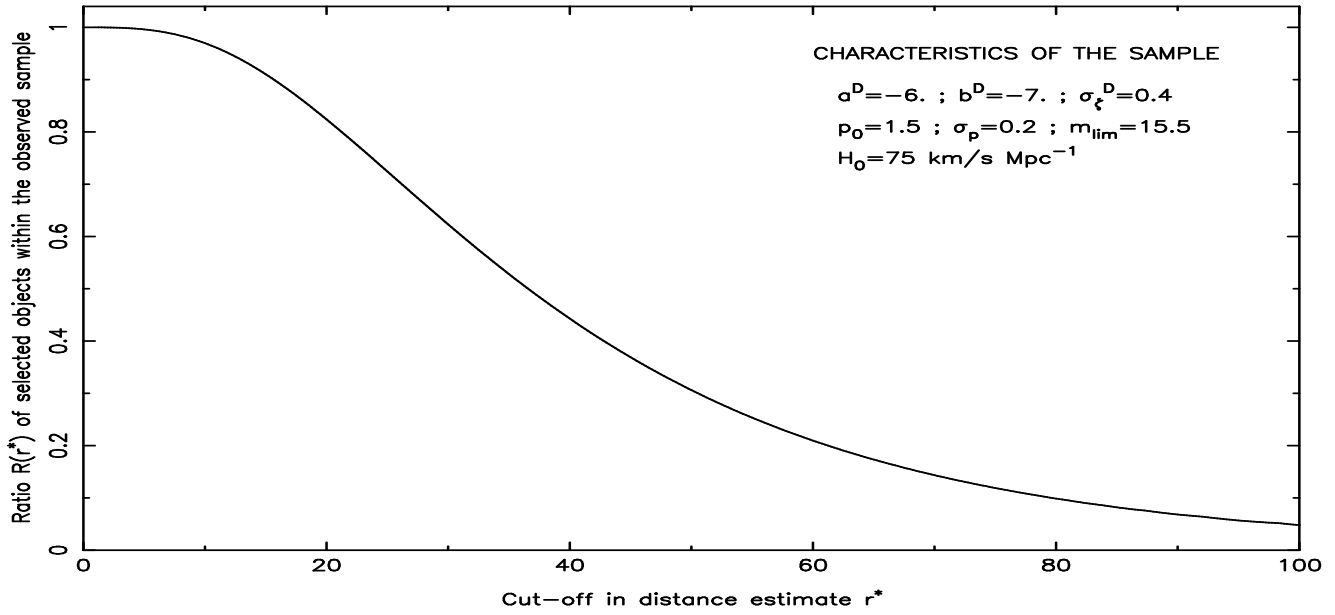


Fig. 1. Variation of the ratio $R(r^*)$ of selected object within the observed sample with respect to the extra cut-off in distance estimate r^* .

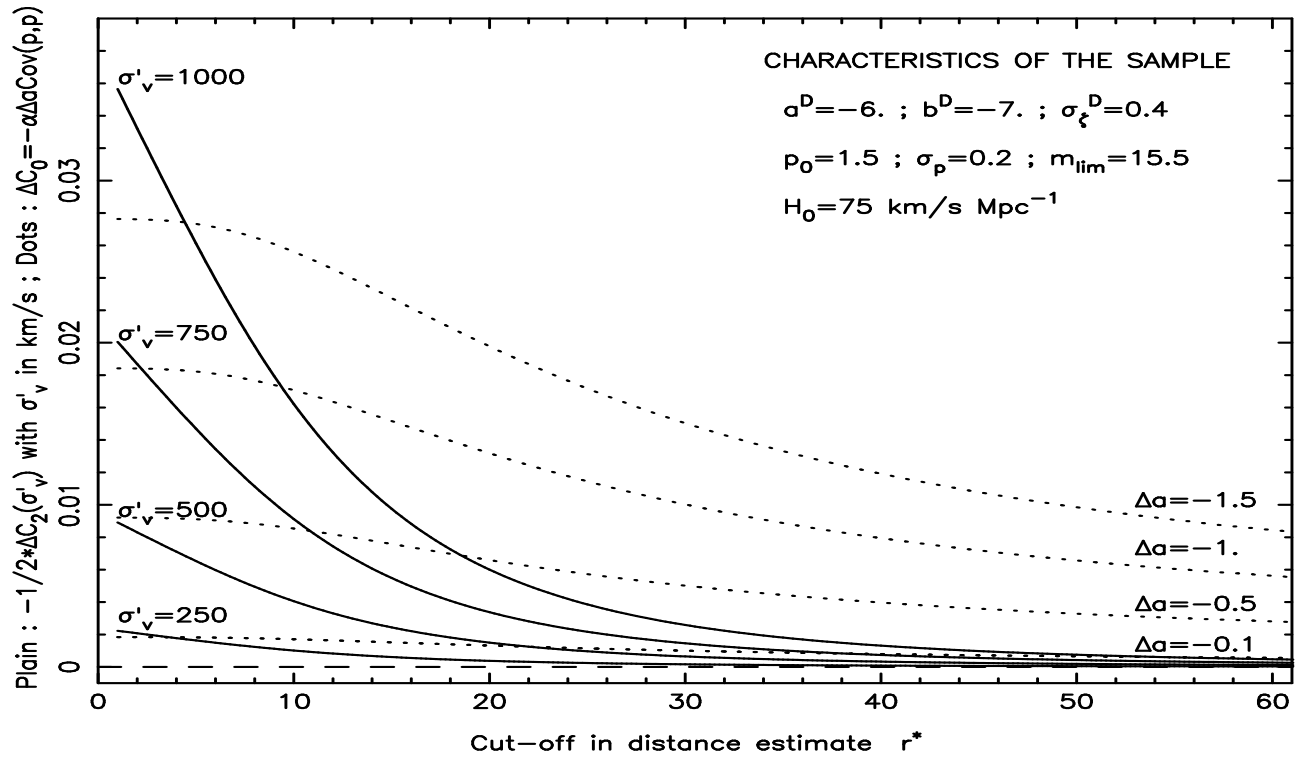


Fig. 2. Variation of the bias ΔC_2 inferred by the presence of a Maxwellian velocity agitation of dispersion σ_v with respect to the extra cut-off in distance estimate r^* ($\sigma'_v = (\sigma_v^2 + u^2)^{1/2}$).

- DTF slope $a^D = -6$.
- DTF zero-point $b^D = -7$.
- DTF intrinsic scatter $\sigma_\zeta^D = 0.4$
- Hubble's constant $H_0 = 75 \text{ km s}^{-1} \text{ Mpc}^{-1}$
- The distribution function of p is a gaussian of mean $p_0 = 1.5$ and dispersion $\sigma_p = 0.2$
- The selection effects in observation restrict to a cut-off in apparent magnitude $m_{\text{lim}} = 15.5$

The two dominant terms of the bias created by the presence of radial peculiar velocities have been calculated (see appendix C for details) :

$$\text{Cov}(p, \ln[1 + \frac{v}{H_0 r}]) = \Delta C_1 - \frac{1}{2} \Delta C_2 + o(\Delta C_2) \quad (19)$$

where the analytical expressions of ΔC_1 and ΔC_2 in function of u , σ_v and r^* can be found Eq. (C11). The amplitude of these terms has to be compared with $\Delta C_0 = -\alpha \Delta a \text{Cov}(p, p)$ appearing in Eq. (14) when a wrong value of the DTF slope is adopted. Expression of ΔC_0 in function of Δa and r^* is given Eq. (C12).

Figure 1 shows variation of $R(r^*)$, i.e. the ratio of selected objects within the observed sample, with respect to the cut-off in distance estimate r^* (analytical expression of $R(r^*)$ is given Eq. (C13)). On one hand, high values of r^* are required in order to minimize as far as possible amplitude of the bias created by radial peculiar velocities. On the other hand, accuracy σ_a of the NCA slope estimate depends on the size of the selected subsample (i.e. $\sigma_a \propto R(r^*)^{-1/2}$ due to the intrinsic statistical fluctuations affecting the sample). Since these two features are indeed competitive (i.e. $R(r^*)$ decreases when r^* increases, compromise on the optimal value of r^* has to be chosen with regard to the specific characteristics of the data sample under consideration).

The variations of term ΔC_2 , i.e. the contribution of a Maxwellian agitation of velocity dispersion σ_v to the bias of Eq. (19), are illustrated Fig. 2. Influence of ΔC_2 on the NCA estimate of the DTF slope a^D given Eq. (15) is obtained by comparing ΔC_2 with the contribution of $\Delta C_0 = -\alpha \Delta a \text{Cov}(p, p)$ to the covariance of Eq. (14). For example, if the mean radial peculiar velocity along the line-of-sight u is zero, the magnitude of the bias on the NCA estimate of a^D created by a velocity field of dispersion $\sigma_v = 1000 \text{ km s}^{-1}$ is greater than $\Delta a = -1.5$ for $r^* = 0$, falls to $\Delta a = -1$ for $r^* \approx 10$ (i.e. $R(r^*) \approx 0.95$), equalizes $\Delta a = -0.5$ for $r^* \approx 20$ (i.e. $R(r^*) \approx 0.8$) and finally falls below $\Delta a = -0.1$ for $r^* \approx 60$ (i.e. $R(r^*) \approx 0.2$). Figure 2 reveals two important features.

- If nearby galaxies are not discarded from the observed sample, the presence of a Maxwellian velocity agitation for galaxies contaminates strongly the NCA estimate of the DTF slope a^D (a velocity dispersion of $\sigma_v = 500 \text{ km s}^{-1}$ induces a bias on a^D of magnitude $\Delta a \approx -0.5$).
- This bias can be rerendered arbitrarily small by selecting only distant galaxies by means of the extra cut-off in distance estimate r^* .

Figure 3 shows the variations of ΔC_1 , i.e. the dominant term of the bias entering Eq. (19) due to the presence of a mean radial peculiar velocity along the line-of-sight u , with respect to r^* . A careful analysis of Fig. 3 leads to the three following remarks.

The term ΔC_1 decreases in function of r^* less rapidly than ΔC_2 . For comparable values of ΔC_1 and ΔC_2 at $r^* = 0$, say for $u = -750 \text{ km s}^{-1}$ and $\sigma_v' = 1000 \text{ km s}^{-1}$, ΔC_1 bias falls to $\Delta a \approx -1.5$ at $r^* = 10$ (to be compared with $\Delta a \approx -1$ for ΔC_2 bias), to $\Delta a \approx -1$ at $r^* = 20$ ($\Delta a \approx -0.5$ for ΔC_2) and finally to $\Delta a \approx -0.5$ at $r^* = 60$ ($\Delta a \approx -0.1$ for ΔC_2). It thus turns out that a particular attention has to be paid in priority to the presence of constant velocity fields.

As the existence of constant velocities strongly biases the NCA estimate of a^D (at $r^* = 0$, $\Delta a \approx -1.3$ for $u = -500 \text{ km s}^{-1}$), discarding nearby galaxies by means of distance estimate selection appears as a quite crucial step. Note however that the situation is not so stringent for samples affected by bulk flow. Since the ΔC_1 bias is antisymmetric with respect to u (see Fig. 3), the bias on the NCA estimate of a^D cancels in average if the opposite line-of-sight direction is also considered. By scanning the sky by line-of-sight directions, this interesting symmetry allows indeed to detect bulk flows already at the level of the calibration step.

Finally, some upper bounds on the a^D bias created by large-scale coherent velocity fields can be extracted from analysis of Fig. 3. Suppose that the line-of-sight of the calibration sample points toward the direction of a Great Attractor, located at a distance estimate of $\tilde{r} = 40 \text{ Mpc}$ and creating back-side infall velocities, say of amplitude $u = -500 \text{ km s}^{-1}$ at $\tilde{r} = 50 \text{ Mpc}$ and slowly decreasing at larger distances. The bias on the NCA estimate of a^D will be necessarily smaller than the ΔC_1 bias for $u = -500 \text{ km s}^{-1}$ (i.e. at $r^* = 50$, $|\Delta a| < 0.5$). This property is closely related to the subsampling in distance estimate allowed by the null-correlation approach. The peculiar velocity field, whatever its specific form, becomes negligible compared to the mean Hubble's flow as long as the cut-off in distance estimate r^* is large enough. In this case the null-correlation approach furnishes unbiased estimate of the DTF slope a^D .

3.2. NCA calibration of the DTF "zero-point" B^*

Assuming that the DTF slope a^D has been correctly calibrated by means of the technique presented section 3.1 or others calibration procedures, the null-correlation approach is herein used for calibrating the remaining calibration parameters entering into the radial peculiar velocity estimator \tilde{v} of Eq. (9). For this purpose, this equation is rewritten as follows :

$$\tilde{v} = z - H_0 \tilde{r} = z - B^* \exp[\alpha(m - a^D p)] \quad (20)$$

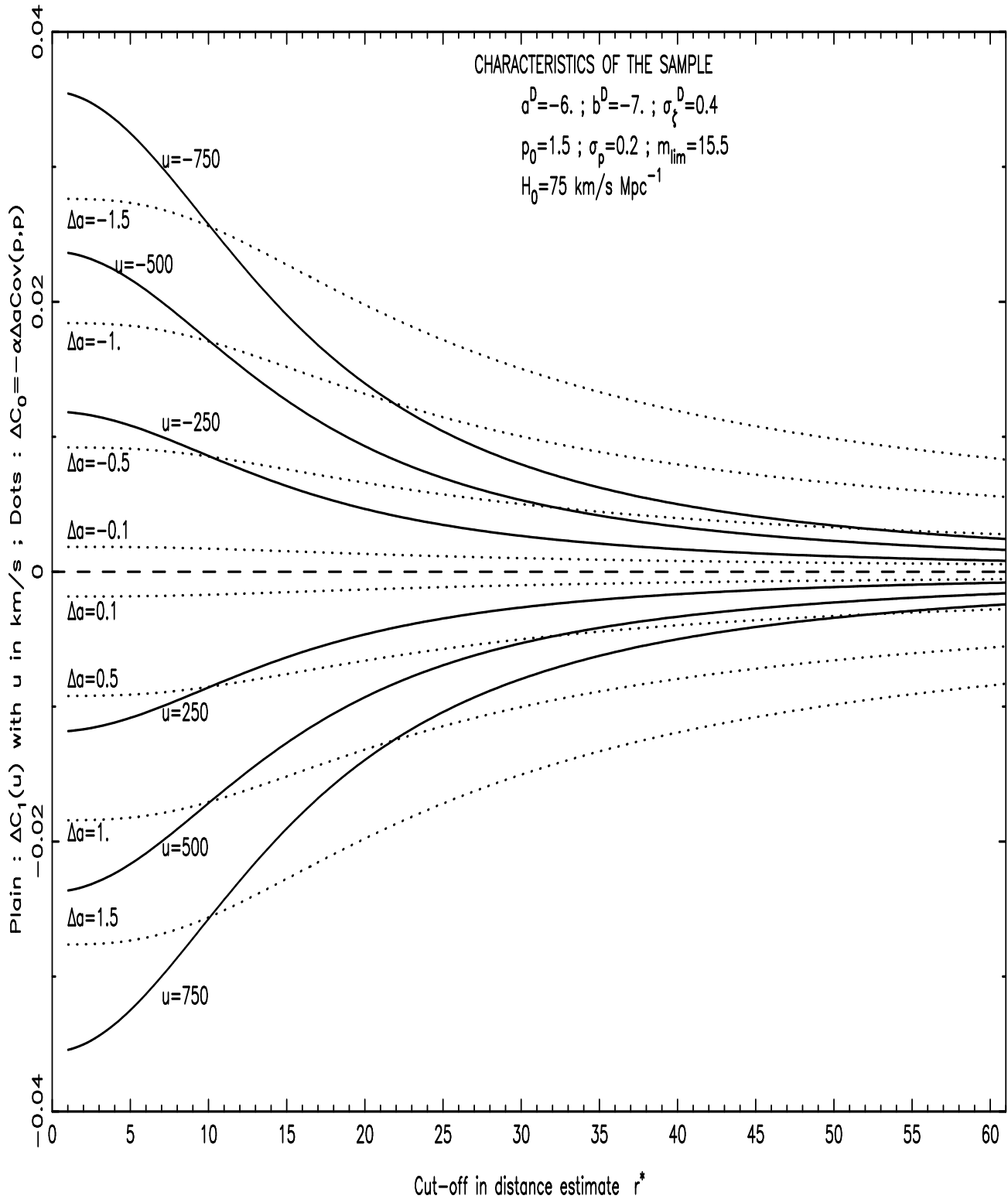


Fig. 3. Variation of the bias ΔC_1 inferred by the presence of a constant velocity u along the line-of-sight with respect to the extra cut-off in distance estimate r^* .

where $B^* = H_0 \exp[\alpha(-b^D - 25)] \exp[\frac{7}{2}\alpha^2 \sigma_\zeta^D 2]$ depends on H_0 , b^D and σ_ζ^D . For a calibration sample satisfying assumptions $\mathcal{H}0$, $\mathcal{H}1$, $\mathcal{H}2$ and $\mathcal{H}3$, the radial peculiar velocity estimator $\tilde{v} = \tilde{v}(a^D, B^*)$ is not correlated with p (see appendix B for proof) :

$$\text{Cov}(p, \tilde{v}) = \text{Cov}(p, \tilde{v}(a^D, B^*)) = 0 \quad (21)$$

On the other hand, a wrong value of the B^* parameter (i.e. $B_F = B^* + \Delta B^*$) correlates p and the random variable $\tilde{v}(a^D, B_F) = z - B_F \exp[\alpha(m - a^D p)]$:

$$\text{Cov}(p, \tilde{v}(a^D, B_F)) = -\frac{\Delta B^*}{B^*} \text{Cov}(p, H_0 \tilde{r}) \neq 0 \quad (22)$$

which does not vanish since selection effects on apparent magnitude m correlate variables p and \tilde{r} (i.e. for selected galaxies, observable p increases in average with the distance estimate \tilde{r}). Assuming that the DTF slope a^D has been correctly calibrated, the NCA estimate of the "zero-point" B^* is then defined as :

$$\text{NCA estimate of } B^* : \beta \text{ such } \text{Cov}(p, \tilde{v}(a^D, \beta)) = 0 \quad (23)$$

which gives in practice :

$$B_*^{\text{NCA}} = \frac{\text{Cov}(p, \exp[\alpha(m - a^D p)])}{\text{Cov}(p, z)} \quad (24)$$

NCA estimate of B^* is clearly robust. It is insensitive to observational selection effects on m and p , specific shape of the luminosity function $f_p(p)$, constant velocity field and Maxwellian agitation of galaxies (see appendix B). Note however that presence of non-constant large scale velocity fields (such GA flow for example) biases NCA estimate of B^* . Unfortunately the subsampling procedure in distance estimate previously proposed is not efficient for dealing with this kind of biases since the contribution of the peculiar velocity v to $\text{Cov}(p, z)$ entering Eq. (24) does not decrease with the distance r .

If one wants to express the distance estimator \tilde{r} of Eq. (6) in true distance units (Mpc), the Hubble's constant H_0 has to be estimated (i.e. $H_0 \tilde{r} = B^* \exp[\alpha(m - a^D p)]$). For this purpose, estimates of the parameters B^* —by using NCA calibration for example—, DTF zero-point b^D —using primary distance indicators— and DTF intrinsic dispersion σ_ζ^D —in galaxies clusters for example— are required (i.e. $H_0 = B^* \exp[\alpha(b^D + 25)] \exp[-\frac{7}{2}\alpha^2 \sigma_\zeta^D 2]$). If B^* is estimated with an error of δB^* , b^D and σ_ζ^D with errors of δb^D and $\delta \sigma_\zeta^D$ respectively, the dominant term of the relative error on the H_0 estimate reads :

$$\frac{\delta H_0}{H_0} \approx \frac{\delta B^*}{B^*} + \alpha \delta b^D - 7\alpha^2 \sigma_\zeta^D \delta \sigma_\zeta^D \quad (25)$$

4. Conclusion

A new technique for calibrating Tully-Fisher like relations was proposed. Based on a null-correlation approach, this calibration procedure is efficient when galaxies constituting the calibration sample are homogeneously distributed in space. The NCA technique is thus adequate for calibrating a sample of field galaxies for example.

In a first step was introduced the random variable $X(a) = \alpha(m - a p) - \ln z$ dependent on a slope parameter a and on the observed apparent magnitude m , log line-width distance indicator p and redshift z . In the case of pure Hubble's flow (i.e. radial peculiar velocities are null everywhere), it was shown that variables p and $X(a)$ are not correlated if and only if parameter a equals the slope a^D of the Direct TF relation. The NCA estimate of the DTF slope a^D was defined as the value of a such that correlation between p and $X(a)$ vanishes. This estimator of a^D was found particularly robust since it does not depend on the selection effects $\phi(m, p)$ on m and p which affect the observed calibration sample and on the specific shape of the luminosity function.

Influences of radial peculiar velocities was investigated in a second step. It was shown that the presence of a peculiar velocity field biases the NCA estimate of a^D . A procedure which consists in discarding nearby galaxies of the observed sample was introduced. Such subsampling is achieved by adding an extra selection function $\psi(m, p)$ in distance estimate \tilde{r} . The magnitude of the bias and its variations in function of the cut-off in distance estimate r^* have been analysed on a synthetic sample and on the Mathewson spirals field galaxies sample (see appendix D). The proposed subsampling procedure looks fairly efficient for minimizing bias on the NCA estimate of the DTF slope a^D created by the presence of radial peculiar velocities.

In the third step, calibration of the "zero-point" parameter B^* entering the definition of the velocity estimator \tilde{v} was investigated. It was shown that the variables p and $\tilde{v}(a^D, \beta) = z - \beta \exp[\alpha(m - a^D p)]$ are not correlated if and only if parameter β equals the "zero-point" B^* . The NCA estimate of the second calibration parameter B^* was thus defined as the value of β such that correlation between p and $\tilde{v}(a^D, \beta)$ vanishes. This B^* estimator is robust. It is insensitive to observational selection effects on m and p and to the specific shape of the luminosity function. Moreover, NCA estimate of B^* is not biased by the presence of a Maxwellian velocity agitation nor by the existence of bulk flow.

Acknowledgements. This work is one of the achievements of a long range program focusing on the statistical modelization of TF like relations, launched five years ago by Roland Triay. He is kindly thanked for constructive discussions. The hospitality of the Centre de Physique Théorique of Luminy is recognized. Stéphane Rauzy is cheerfully thanked for a generous financial support.

A. The distance estimator \tilde{r}

The probability density dP_{m_o, p_o} describing a sample of galaxies with the same observed m_o and p_o can be derived from Eq. (5) by using conditional probability :

$$dP_{m_o, p_o} = \frac{1}{A_{m_o, p_o}} \delta(m - m_o) \delta(p - p_o) \phi(m, p) f_p(p) dp g(\zeta^D; 0, \sigma_\zeta^D) d\zeta^D h(\mu) d\mu \quad (\text{A1})$$

where δ is the Dirac distribution (i.e. $\int \delta(x - x_0) f(x) dx = f(x_0)$) and the normalisation factor A_{m_o, p_o} reads :

$$A_{m_o, p_o} = \int \delta(m - m_o) \delta(p - p_o) \phi(m, p) f_p(p) dp g(\zeta^D; 0, \sigma_\zeta^D) d\zeta^D h(\mu) d\mu \quad (\text{A2})$$

If the two following hypotheses are verified by the sample :

- $\mathcal{H}1$) $g(\zeta^D; 0, \sigma_\zeta^D)$ is gaussian, i.e. $g \equiv g_G$ with $g_G(x; x_0, \sigma) = (\sqrt{2\pi} \sigma)^{-1} \exp[-(x - x_0)^2/(2\sigma^2)]$.
- $\mathcal{H}2$) Galaxies are homogeneously distributed along the line-of-sight, i.e. $h(\mu) = \exp[3\alpha\mu]$ with $\alpha = \frac{\ln 10}{5}$.

the successive integrations over m , p and ζ^D give for the normalisation factor A_{m_o, p_o} :

$$A_{m_o, p_o} = \phi(m_o, p_o) f_p(p_o) \exp[3\alpha(m_o - a^D p_o - b^D)] \exp[\frac{9}{2}\alpha^2 \sigma_\zeta^D 2] \quad (\text{A3})$$

where the properties (A4) and (A5a) of gaussian functions have been used :

$$\exp[\lambda x] g_G(x; x_0, \sigma) = \exp[\lambda(x_0 + \lambda\sigma^2/2)] g_G(x; x_0 + \lambda\sigma^2, \sigma) \quad (\text{A4})$$

$$\int g_G(x; x_0, \sigma) dx = 1 \quad (\text{a}) \quad ; \quad \int x g_G(x; x_0, \sigma) dx = x_0 \quad (\text{b}) \quad ; \quad \int x^2 g_G(x; x_0, \sigma) dx = \sigma^2 + x_0^2 \quad (\text{c}) \quad (\text{A5})$$

By using property (A4) and Eq. (A3), the distribution of distance modulus μ for the sample rewrites thus :

$$dP_{m_o, p_o} = g_G(\mu; m_o - a^D p_o - b^D + 3\alpha \sigma_\zeta^D 2, \sigma_\zeta^D) d\mu \quad (\text{A6})$$

Properties (A4) and (A5a) imply that the mathematical expectancy $E(r)$ of the distance $r = \exp[\alpha(\mu - 25)]$ reads :

$$E(r) = \int r dP_{m_o, p_o} = \exp[\alpha(m_o - a^D p_o - b^D - 25)] \exp[\frac{7}{2}\alpha^2 \sigma_\zeta^D 2] \quad (\text{A7})$$

This quantity is generally chosen as distance estimator \tilde{r} of individual galaxy with measured m_o and p_o . Note however that others estimators could be used, such as the most likely value of the distance r which does not coincide with $E(r)$ since the probability density function (*pdf*) of the variable r is lognormal, and so not symmetric around its mean. The accuracy $\Delta\tilde{r}$ of the distance estimator \tilde{r} can be derived from Eqs. (A6,A7) by using properties (A4) and (A5a) :

$$\Delta\tilde{r} = \sqrt{E((r - \tilde{r})^2)} = \tilde{r} \sqrt{\exp[\alpha^2 \sigma_\zeta^D 2] - 1} \quad (\text{A8})$$

B. Correlation between p and \tilde{v}

Hereafter, the correlation between p and the velocity estimator \tilde{v} given Eq. (20) is calculated assuming the following hypothesis :

- $\mathcal{H}3$) Along a line-of-sight, the distribution of radial peculiar velocities v does not depend on distances r and is a gaussian of mean u and dispersion σ_v , i.e. $f_v(v; \mathbf{x}) = g_G(v; u, \sigma_v)$.

Under assumptions $\mathcal{H}1$, $\mathcal{H}2$ and $\mathcal{H}3$, the probability density dP_3 of Eq. (11) rewrites :

$$dP_3 = \frac{1}{A_3} \phi(m, p) f_p(p) dp g_G(\zeta^D; 0, \sigma_\zeta^D) d\zeta^D \exp[3\alpha\mu] d\mu g_G(v; u, \sigma_v) dv \quad (\text{B1})$$

In order to calculate each term involved in the covariance of p and \tilde{v} , i.e. $\text{Cov}(p, \tilde{v}) = E(p\tilde{v}) - E(p)E(\tilde{v})$, the velocity estimator \tilde{v} given Eq. (9) is rewritten in terms of variables v , ζ^D and μ :

$$\tilde{v} = v + H_0 \exp[\alpha(\mu - 25)] \left[1 - \exp[-\alpha\zeta^D] \exp[\frac{7}{2}\alpha^2 \sigma_\zeta^D 2] \right] \quad (\text{B2})$$

Since u is a constant, $\text{Cov}(p, \tilde{v} - u) = E(p(\tilde{v} - u)) - E(p)E(\tilde{v} - u) = \text{Cov}(p, \tilde{v})$. Integrating over the variable v gives for the three quantities $E(p) = \int p dP_3$, $E(\tilde{v} - u) = \int (\tilde{v} - u) dP_3$ and $E(p(\tilde{v} - u)) = \int p(\tilde{v} - u) dP_3$:

$$E(p) = \frac{1}{A_3} \int \phi(m, p) p f_p(p) dp g_G(\zeta^D; 0, \sigma_\zeta^D) d\zeta^D h(\mu) d\mu \quad (\text{B3})$$

$$E(\tilde{v} - u) = \frac{1}{A_3} \int \phi(m, p) f_p(p) dp g_G(\zeta^D; 0, \sigma_\zeta^D) d\zeta^D h(\mu) d\mu H_0 \exp[\alpha(\mu - 25)] \left[1 - \exp[-\alpha\zeta^D] \exp[\frac{7}{2}\alpha^2\sigma_\zeta^{D2}] \right] \quad (\text{B4})$$

$$E(p(\tilde{v} - u)) = \frac{1}{A_3} \int \phi(m, p) p f_p(p) dp g_G(\zeta^D; 0, \sigma_\zeta^D) d\zeta^D h(\mu) d\mu H_0 \exp[\alpha(\mu - 25)] \left[1 - \exp[-\alpha\zeta^D] \exp[\frac{7}{2}\alpha^2\sigma_\zeta^{D2}] \right] \quad (\text{B5})$$

where properties (A5a) and (A5b) have been used. Replacing $h(\mu)$ by $\exp[3\alpha\mu] = \exp[3\alpha(m - a^D p - b^D + \zeta^D)]$ and using definition of B given Eq. (9), Eqs. (B3,B4,B5) expressed in terms of p , m and ζ^D read :

$$E(p) = \frac{1}{A_3} \int \phi(m, p) p f_p(p) \exp[3\alpha(m - a^D p - b^D)] dm dp \times \int \exp[3\alpha\zeta^D] g_G(\zeta^D; 0, \sigma_\zeta^D) d\zeta^D \quad (\text{B6})$$

$$E(\tilde{v} - u) = \frac{B}{A_3} \int \phi(m, p) f_p(p) \exp[4\alpha(m - a^D p - b^D)] dm dp \times C \quad (\text{B7})$$

$$E(p(\tilde{v} - u)) = \frac{B}{A_3} \int \phi(m, p) p f_p(p) \exp[4\alpha(m - a^D p - b^D)] dm dp \times C \quad (\text{B8})$$

where the constant C is defined as follows :

$$C = \int \left[\exp[4\alpha\zeta^D] - \exp[3\alpha\zeta^D] \exp[\frac{7}{2}\alpha^2\sigma_\zeta^{D2}] \right] g_G(\zeta^D; 0, \sigma_\zeta^D) d\zeta^D \quad (\text{B9})$$

By using properties (A4) and (A5a), it is found that integral of Eq. (B9) vanishes. It thus implies that $C = 0$, $E(\tilde{v} - u) = 0$, $E(p(\tilde{v} - u)) = 0$, $\text{Cov}(p, \tilde{v} - u) = 0$ and finally $\text{Cov}(p, \tilde{v}) = 0$. This result does not depend on the shape of the selection function $\phi(m, p)$ in m and p , on the theoretical distribution function $f_p(p)$ of the variable p and on the mean radial peculiar velocity u along the line-of-sight. For a sample of galaxies satisfying hypotheses $\mathcal{H}1$, $\mathcal{H}2$ and $\mathcal{H}3$, it thus turns out that the observable p is not correlated with the velocity estimator \tilde{v} as long as the model parameters entering into $\tilde{v} = \tilde{v}(a^D, b^D, \sigma_\zeta^D, H_0)$ via Eq. (9) are correct². On the other hand, if a wrong value is assumed for one of these calibration parameters, say for example that a^D , b^D and σ_ζ^D are correct but not the Hubble's constant $H_F = H_0 + \Delta H_0$, the covariance between p and $v_F = \tilde{v}(a^D, b^D, \sigma_\zeta^D, H_F)$ gives :

$$\text{Cov}(p, v_F) = \text{Cov}(p, \tilde{v} - \Delta H_0 \tilde{r}) = 0 - \Delta H_0 \text{Cov}(p, \tilde{r}) \neq 0 \quad (\text{B10})$$

which does not vanish since existing selection effects on apparent magnitude m correlate variables p and \tilde{r} (i.e. for selected galaxies, observable p increases in average with the distance estimator \tilde{r}). This point motivates the use of a null-correlation approach³ in order to calibrate Tully-Fisher like relations.

C. Correlation between p and X

In this appendix, the reliability of null-correlation approach in order to estimate the slope a^D of the DTF relation is discussed. In a first step, it is shown that the non-observable variable $X_0 = X_0(a^D) = \alpha(m - a^D p) - \ln[H_0 r]$ is not correlated with p as long as hypotheses $\mathcal{H}1$ and $\mathcal{H}2$ are satisfied. Particularly, this property does not depend on the selection function on m and p . In a second step, the correlation between p and the observable variable X :

$$X = X(a^D) = \alpha(m - a^D p) - \ln z = X_0 - \ln[1 + \frac{v}{H_0 r}] \quad (\text{C1})$$

² Note however that the converse does not hold since the Hubble's constant H_0 , DTF zero-point b^D and intrinsic DTF dispersion σ_ζ^D degenerate into a single parameter $B^* = H_0 \exp[-\alpha(b^D + 25)] \exp[\frac{7}{2}\alpha^2\sigma_\zeta^{D2}]$.

³ It can be proven similarly that $\text{Cov}(m, \tilde{v}) = 0$.

is investigated. The presence of radial peculiar velocities such as the ones assumed in $\mathcal{H}3$ indeed correlates p and X . However, it is shown that the amplitude of this effect can be weakened by selecting only distant galaxies of the sample. It is not surprising since the term $\ln[1 + v/(H_0 r)]$ in Eq. (C1) becomes negligible for distances r large enough. Such a subsampling can be performed by discarding galaxies of the observed sample which have a distance estimate \tilde{r} less than a given r^* . It corresponds to introduce an extra selection function $\psi(m, p)$ defined as follows :

$$\psi(m, p) = 1 \text{ if } \tilde{r} = \exp[\alpha(m - a^D p - b^D - 25)] \exp[\frac{7}{2}\alpha^2\sigma_\zeta^{D,2}] \geq r^* ; \quad \psi(m, p) = 0 \text{ otherwise.} \quad (\text{C2})$$

Note that introducing this extra selection effect does not alter the result $\text{Cov}(p, X_0) = 0$. On the other hand, a wrong value of the DTF slope (i.e. $a_F = a^D + \Delta a$) correlates p and $X(a_F) = \alpha(m - a_F p) - \ln z$:

$$\text{Cov}(p, X(a_F)) = \text{Cov}(p, X_0(a_F)) + \text{Cov}(p, -\ln[1 + \frac{v}{H_0 r}]) = -\alpha\Delta a \text{Cov}(p, p) - \text{Cov}(p, \ln[1 + \frac{v}{H_0 r}]) \neq 0 \quad (\text{C3})$$

where $\text{Cov}(p, p) = E([p - E(p)]^2) = \Sigma(p)^2$ is the square of standard deviation of p . The null-correlation approach thus consists to adopt the value of the parameter a verifying $\text{Cov}(p, X(a)) = 0$ as the correct estimate of the slope a^D of the DTF relation.

It is proven below that $\text{Cov}(p, X_0 = \alpha(m - a^D p) - \ln[H_0 r]) = 0$ as long as assumptions $\mathcal{H}1$ and $\mathcal{H}2$ are satisfied by the sample. Rewriting the non-observable variable X_0 in terms of m , p and μ gives $X_0 = \alpha(m - a^D p - \mu + 25) - \ln H_0$. In terms of ζ^D , it reads $X_0 = -\alpha\zeta^D - \ln B$ where $B = H_0 \exp[\alpha(-b^D - 25)]$ was previously defined Eq. (9). Since α and $\ln B$ are constants, $\text{Cov}(p, X_0) = -\alpha \text{Cov}(p, \zeta^D)$. The null-correlation between p and ζ^D can be shown by replacing $h(\mu)$ by $\exp[3\alpha\mu] = \exp[3\alpha(m - a^D p - b^D + \zeta^D)]$ and using the probability density dP_2 of Eq. (5) expressed in terms of p , m and ζ^D :

$$E(p) = \frac{1}{A_2} Q_1 \times Q_2 = \frac{1}{A_2} \int \phi(m, p) p f_p(p) \exp[3\alpha(m - a^D p - b^D)] dm dp \times \int \exp[3\alpha\zeta^D] g_G(\zeta^D; 0, \sigma_\zeta^D) d\zeta^D \quad (\text{C4})$$

$$E(\zeta^D) = \frac{1}{A_2} Q_3 \times Q_4 = \frac{1}{A_2} \int \phi(m, p) f_p(p) \exp[3\alpha(m - a^D p - b^D)] dm dp \times \int \zeta^D \exp[3\alpha\zeta^D] g_G(\zeta^D; 0, \sigma_\zeta^D) d\zeta^D \quad (\text{C5})$$

$$E(p\zeta^D) = \frac{1}{A_2} Q_1 \times Q_4 = \frac{1}{A_2} \int \phi(m, p) p f_p(p) \exp[3\alpha(m - a^D p - b^D)] dm dp \times \int \zeta^D \exp[3\alpha\zeta^D] g_G(\zeta^D; 0, \sigma_\zeta^D) d\zeta^D \quad (\text{C6})$$

where the normalisation factor A_2 reads :

$$A_2 = Q_3 \times Q_2 = \int \phi(m, p) f_p(p) \exp[3\alpha(m - a^D p - b^D)] dm dp \times \int \exp[3\alpha\zeta^D] g_G(\zeta^D; 0, \sigma_\zeta^D) d\zeta^D \quad (\text{C7})$$

It thus turns out that $\text{Cov}(p, \zeta^D) = E(p\zeta^D) - E(p)E(\zeta^D) = (A_2)^{-2} [A_2 Q_1 Q_4 - Q_1 Q_2 \times Q_3 Q_4] = 0$, which implies $\text{Cov}(p, X_0) = 0$. This result⁴ is insensitive to the shape of the selection function $\phi(m, p)$ in m and p and to the theoretical distribution function $f_p(p)$ of the variable p .

The term $\text{Cov}(p, \ln[1 + v/(H_0 r)])$ entering into Eq. (C3) does not vanish since p is correlated with distance r . However, its amplitude can be rerendered arbitrarily small by adding an extra selection effect such as the one mentioned Eq. (C2). This feature is illustrated by the following example. It is assumed that :

- Hypotheses $\mathcal{H}1$, $\mathcal{H}2$ and $\mathcal{H}3$ are satisfied by the sample.
- The distribution function of p is a gaussian of mean p_0 and dispersion σ_p (i.e. $f_p(p) = g_G(p; p_0, \sigma_p)$).
- The selection effects in observation restrict to a cut-off in apparent magnitude (i.e. $\phi(m, p) \equiv \phi_m(m) = \theta(m_{\text{lim}} - m)$ where θ is the Heaveside distribution function, $\theta(x) = 1$ if $x \geq 0$ and $\theta(x) = 0$ otherwise).

The subsampling is performed by using the extra selection function $\psi(m, p)$ proposed Eq. (C2). By introducing μ^* such that $r^* = \exp[\alpha(\mu^* - 25)] \exp[\frac{7}{2}\alpha^2\sigma_\zeta^{D,2}]$, ψ rewrites $\psi(m, p) = \theta([m - a^D p - b^D] - \mu^*)$. Adding this extra selection function $\psi(m, p)$, the probability density dP_3 of Eq. (11) reads :

$$dP_4 = \frac{1}{A_4} \theta(m_{\text{lim}} - m) \theta([m - a^D p - b^D] - \mu^*) g_G(p; p_0, \sigma_p) dp g_G(\zeta^D; 0, \sigma_\zeta^D) d\zeta^D \exp[3\alpha\mu] d\mu g_G(v; u, \sigma_v) dv \quad (\text{C8})$$

⁴ It can be proven similarly that $\text{Cov}(m, X_0) = 0$.

Since the probability density dP_4 describing the sample is fully specified, calculations of quantities of interest can be performed analytically or by using numerical simulations. Hereafter, cumbersome intermediate calculations have been deliberately omitted and we just furnish the ultimate analytical expressions of these quantities.

In order to evaluate the amplitude of the term $\text{Cov}(p, \ln[1 + v/(H_0 r)])$ entering Eq. (C3), $\ln[1 + v/(H_0 r)]$ is expanded in Taylor's series up to order 2 :

$$\ln(1 + \frac{v}{H_0 r}) = \frac{v}{H_0 r} - \frac{1}{2} \frac{v^2}{H_0^2 r^2} + \circ \left(\frac{v^2}{H_0^2 r^2} \right) \quad (\text{C9})$$

It implies that the covariance may be expanded as follows :

$$\text{Cov}(p, \ln[1 + \frac{v}{H_0 r}]) = \Delta C_1 - \frac{1}{2} \Delta C_2 + \circ(\Delta C_2) = \text{Cov}(p, \frac{v}{H_0 r}) - \frac{1}{2} \text{Cov}(p, \frac{v^2}{H_0^2 r^2}) + \circ \left(\text{Cov}(p, \frac{v^2}{H_0^2 r^2}) \right) \quad (\text{C10})$$

The calculations give for the terms ΔC_1 and ΔC_2 :

$$\Delta C_1 = \frac{u}{H_0} \left(\frac{J[\mu^*; 2]}{I[\mu^*; 3]} - \frac{J[\mu^*; 3]}{I[\mu^*; 3]} \frac{I[\mu^*; 2]}{I[\mu^*; 3]} \right) \quad (\text{a}) \quad ; \quad \Delta C_2 = \frac{u^2 + \sigma_v^2}{H_0^2} \left(\frac{J[\mu^*; 1]}{I[\mu^*; 3]} - \frac{J[\mu^*; 3]}{I[\mu^*; 3]} \frac{I[\mu^*; 1]}{I[\mu^*; 3]} \right) \quad (\text{b}) \quad (\text{C11})$$

where the functions $I[\mu^*; N]$ and $J[\mu^*, N]$ are defined Eq. (C14) and Eq. (C15). For a given cut-off in distance estimate μ^* , the contribution of ΔC_1 and ΔC_2 to $\text{Cov}(p, X)$ has to be compared with $\Delta C_0 = -\alpha \Delta a \text{Cov}(p, p)$ appearing in Eq. (C3) when a wrong value of the DTF slope is adopted. This term ΔC_0 reads :

$$\Delta C_0 = -\alpha \Delta a \text{Cov}(p, p) = -\alpha \Delta a \left(\frac{H[\mu^*]}{I[\mu^*; 3]} - \frac{J[\mu^*; 3]^2}{I[\mu^*; 3]^2} \right) \quad (\text{C12})$$

where the function $H[\mu^*]$ is defined Eq. (C19) and $I[\mu^*; 3]$ and $J[\mu^*, 3]$ Eqs. (C14,C15). Finally, the last quantity of interest is the ratio $R(\mu^*)$ of selected objects within the observed sample. This ratio is equal to the normalisation factor $A_4(\mu^*) = I(\mu^*; 3)$ divided by $A_4(\mu^* \rightarrow -\infty)$, i.e. the normalisation factor of the sample when no extra selection effect is present ($r^* = 0$ or $\mu^* \rightarrow -\infty$). It reads in function of the extra cut-off in distance estimate μ^* introduced Eq. (C8) as follows :

$$R(\mu^*) = \mathcal{M}_0(\omega[\mu^*; 3]) - \mathcal{M}_0(\omega[\mu^*; 0]) \exp[3\alpha(\mu^* + a^D p_0 + b^D - m_{\text{lim}} + \frac{3}{2}\alpha a^{D 2} \sigma_p^2)] \quad (\text{C13})$$

where $\omega[\mu^*; N]$ is defined Eq. (C18) and the $\mathcal{M}_0(x)$ function is introduced Eq. (C17).

NOTATIONS :

$I[\mu^*; N]$ and $J[\mu^*, N]$, function of the extra cut-off μ^* and of an integer N , are defined as follows :

$$I[\mu^*; N] = K[N] \left(\mathcal{M}_0(\omega[\mu^*; N]) - \mathcal{M}_0(\omega[\mu^*; 0]) \exp[N\alpha(\mu^* + a^D p_0 + b^D - m_{\text{lim}} - \frac{N}{2}\alpha a^{D 2} \sigma_p^2)] \right) \quad (\text{C14})$$

$$\begin{aligned} J[\mu^*; N] = & +K[N] (\sigma_p \mathcal{M}_1(\omega[\mu^*; N]) + (p_0 - N\alpha a^D \sigma_p^2) \mathcal{M}_0(\omega[\mu^*; N])) \\ & -K[N] (\sigma_p \mathcal{M}_1(\omega[\mu^*; 0]) + p_0 \mathcal{M}_0(\omega[\mu^*; 0])) \exp[N\alpha(\mu^* + a^D p_0 + b^D - m_{\text{lim}} - \frac{N}{2}\alpha a^{D 2} \sigma_p^2)] \end{aligned} \quad (\text{C15})$$

where $K(N)$, function of an integer N , is :

$$K[N] = \frac{1}{N\alpha} \exp[N\alpha(m_{\text{lim}} - a^D p_0 - b^D - 25 + \frac{N}{2}\alpha(a^{D 2} \sigma_p^2 + \sigma_{\zeta}^{D 2}))] \quad (\text{C16})$$

$\mathcal{M}_0(x)$, $\mathcal{M}_1(x)$ and $\mathcal{M}_2(x)$ functions reads :

$$N(t) = g_G(t; 0, 1) \quad ; \quad \mathcal{M}_0(x) = \int_x^{+\infty} N(t) dt \quad ; \quad \mathcal{M}_1(x) = \int_x^{+\infty} t N(t) dt \quad ; \quad \mathcal{M}_2(x) = \int_x^{+\infty} t^2 N(t) dt \quad (\text{C17})$$

and $\omega[\mu^*; N]$, function of the extra cut-off μ^* and of an integer N , is :

$$\omega[\mu^*; N] = \frac{m_{\text{lim}} - a^D p_0 - b^D - \mu^* + N\alpha a^{D 2} \sigma_p^2}{a^D \sigma_p} \quad (\text{C18})$$

The function $H[\mu^*]$, involved in the calculation of $\text{Cov}(p, p)$, is defined as follows :

$$\begin{aligned} \frac{H[\mu^*]}{K[3]} = & -(\sigma_p^2 \mathcal{M}_2(\omega[\mu^*; 0]) + 2\sigma_p p_0 \mathcal{M}_1(\omega[\mu^*; 0]) + p_0^2 \mathcal{M}_0(\omega[\mu^*; 0])) \exp[3\alpha(\mu^* + a^D p_0 + b^D - m_{\text{lim}} + \frac{3}{2}\alpha a^D \sigma_p^2)] \\ & + \sigma_p^2 \mathcal{M}_2(\omega[\mu^*; 3]) + 2\sigma_p(p_0 - 3\alpha a^D \sigma_p^2) \mathcal{M}_1(\omega[\mu^*; 3]) + (p_0 - 3\alpha a^D \sigma_p^2)^2 \mathcal{M}_0(\omega[\mu^*; 3]) \end{aligned} \quad (\text{C19})$$

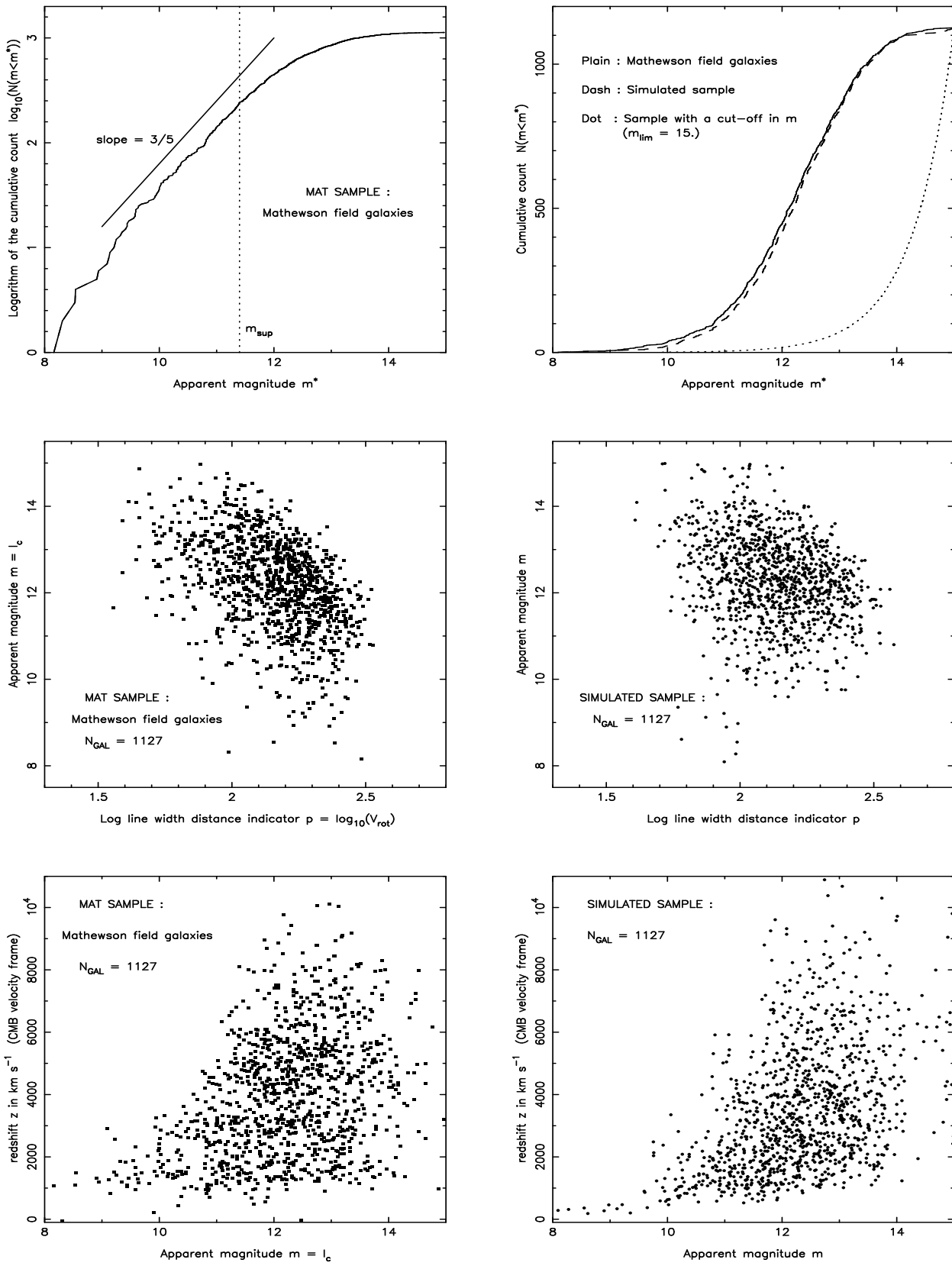


Fig. 4. Mathewson spiral field galaxies sample versus simulated sample.

D. Application to the Mathewson field galaxies sample

The spiral field galaxies sample of Mathewson et al. 1992 is a composite sample of $N_{\text{gal}} = 1127$ spiral galaxies lying in the field (galaxies identified as cluster members have been excluded of this catalog). It covers the south hemisphere and extends in redshift up to $10\,000 \text{ km s}^{-1}$ with an effective depth of about $4\,000 \text{ km s}^{-1}$. Selection effects in observation are not trivial to model since sampled galaxies have been firstly selected in apparent diameter before Mathewson et al. apply their own selection criteria (minimum limits in inclination and velocity rotation). Some galaxies inherited from others observational programs have been also included in the sample. The data used hereafter in the analysis are :

- the apparent magnitude $m = I_t^c$ where I_t^c is the total I-band apparent magnitude corrected for internal and external extinction and K-dimming (column (6), second row in Mathewson et al. 1992).
- the log line-width distance indicator $p = \log_{10} V_{\text{rot}}$ where V_{rot} is the maximum velocity of rotation of the spiral galaxy (column (9) in Mathewson et al. 1992).
- the redshift $z = V_{\text{CMB}}$ in km s^{-1} unit expressed in the CMB velocity frame (column (11), first row in Mathewson et al. 1992).

The application is presented as follows. In section D.1 is explained how numerical simulations, used throughout the analysis for quantifying the amplitude of errors bars and velocity biases, are performed. Section D.2 is devoted to test on the calibration parameters proposed by Mathewson et al. 1992. Finally, NCA calibration of the Mathewson field galaxies sample is performed section D.3.

D.1. Accuracies, amplitude of biases and simulations

Accuracies of the NCA calibration parameter estimators are herein calculated by using numerical simulations. Reliability of the values of such standard deviations is of course closely related to the way simulated samples succeed in reproducing the characteristics of the real sample under consideration. A preliminar study of the Mathewson field galaxies (MAT) sample characteristics is thus required.

On figure 4 (top left) is shown the decimal logarithm of the cumulative count in function of the apparent magnitude m for the MAT sample. It turns out that the completeness in magnitude of the MAT sample is violated beyond $m_{\text{sup}} = 11.3$, corresponding to about 1/5 of the total number of sampled galaxies. Observational selection effects are then more complex than a mere cut-off m_{lim} in apparent magnitude. In order to mimic the real selection effects in observation affecting the MAT sample, simulations are built in two steps.

A virtual sample, complete in apparent magnitude up to $m_{\text{lim}} = 15$., is firstly generated assuming the following

characteristics :

- Variable p is generated according to a gaussian distribution function $f_p(p) = g_G(p; p_0, \sigma_p)$.
- Variable ζ^D , accounting for the intrinsic scatter of the DTF relation, is generated according to a gaussian distribution function $g_G(\zeta^D; 0, \sigma_{\zeta}^D)$.
- The absolute magnitude $M = a^D p + b^D - \zeta^D$ is then formed, with a^D and b^D the slope and the zero-point of the DTF relation.
- Variable μ is generated according to an exponential distribution function $h(\mu) = \exp(3\alpha\mu)$ and such that $\mu < m_{\text{lim}} - M$ (i.e. distances are thus uniformly distributed in space).
- The redshift $z = H_0 \exp[\alpha(\mu - 25)]$ with H_0 the Hubble's constant in $\text{km s}^{-1} \text{ Mpc}^{-1}$ is finally formed according to the pure Hubble's flow hypothesis.

Adopted values for the parameters p_0 , σ_p , σ_{ζ}^D , a^D , b^D and H_0 , as well as their corresponding "zero-points" B and B^* introduced Eqs. (9,20), are given table 1.

The next step is to extract from this virtual sample a subsample of $N_{\text{gal}} = 1127$ which has the same distribution in m and p than the observed distribution of the MAT sample. In effect this selection is achieved as follows. The m - p plane is divided in boxes $box(i)$ of equal size and the number $n(i)$ of MAT galaxies belonging to each box $box(i)$ is memorized. Boxes $box(i)$ are afterwards filled with galaxies belonging to the virtual sample while the observed $n(i)$ are not reached. This selection procedure ensures that the m - p distribution of the simulated samples is approximately identical to the observed one. It corresponds to introduce a complex selection function $\phi_{\text{MAT}}(m, p)$ in m and p directly derived from the data.

Table 1. Adopted values for the parameters of the simulations

p_0	σ_p	σ_{ζ}^D	a^D	b^D	H_0	B	B^*
1.82	0.2	0.35	-7.	-5.3	85	0.0097	0.0106

Figure 4 (top right) shows the cumulative count in apparent magnitude for the MAT sample and for a simulated sample. The cumulative count expected for a sample complete up to $m_{\text{lim}} = 15$. is also shown for comparison. Figures 4 (center left) and (center right) show respectively the distribution in the m - p plane of the MAT sample and a simulated sample. The difference between these two distributions are due to discretization effects which appear when applying the boxes algorithm. Figures 4 (bottom left) and (bottom right) show respectively the m - z distributions for the MAT sample and for a simulated sample. The fact that simulated sample distribution approximately reproduces the observed one is encourag-

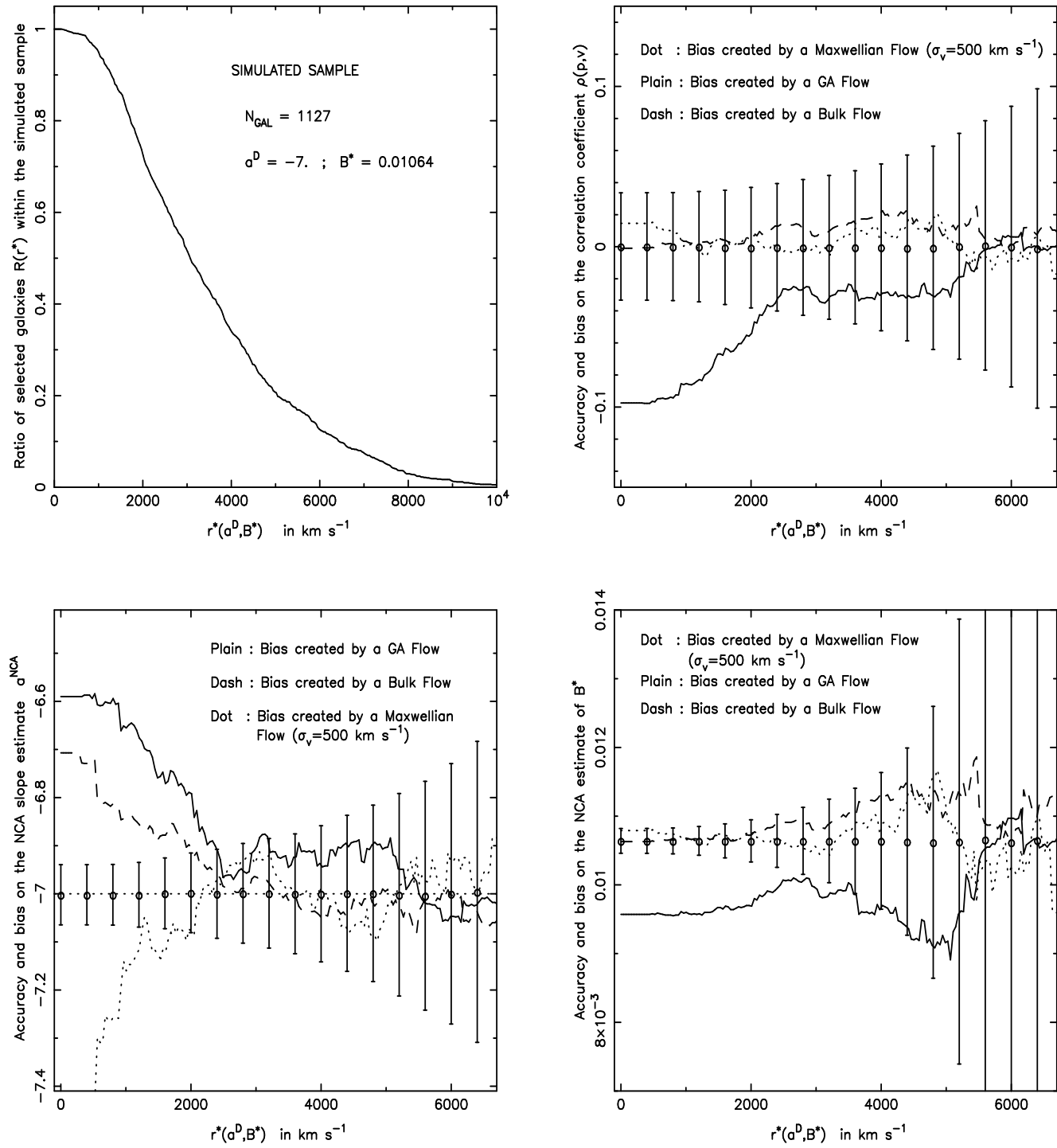


Fig. 5. Accuracies of NCA estimators and amplitudes of velocity biases : (Top left) Ratio $R(r^*)$ of selected galaxies within the simulated samples function of the extra cut-off in distance estimate $r^*(a^D, B^*)$. (Top right) Standard deviation for the correlation coefficient $\rho(p, \tilde{v})$ and velocity biases created by GA, Bulk and Maxwellian flows. (Bottom left) Standard deviation for NCA slope estimator a^{NCA} and velocity biases created by GA, Bulk and Maxwellian flows. (Bottom right) Standard deviation for NCA "zero-point" estimator B^{NCA} and velocity biases created by GA, Bulk and Maxwellian flows.

ing. It means that the working hypotheses assumed when generating simulated samples, such as the uniform spatial distribution of galaxies, are close to be verified by the Mathewson field galaxies sample. The likeness to data can certainly be improved, by choosing a more realistic shape for the luminosity function for example (i.e. the p distribution $f_p(p)$), but is out of the scope of this study. Hereafter, these simulated samples will be considered as fair representatives of the observed catalog.

Figure 5 visualizes results obtained on these simulated samples. At the top left is plotted the ratio $R(r^*)$ of selected galaxies within a simulated sample when the subsampling in distance estimate (i.e. $\tilde{r} > r^*(a^D, B^*)$) is applied. Standard statistical deviation of the correlation coefficient between p and the velocity estimates $\tilde{v}(a^D, B^*)$ in function of the cut-off in distance estimate r^* is shown figure 5 (top right). Standard deviation (i.e. accuracy) of the NCA slope estimator a^{NCA} and of the NCA "zero-point" B_*^{NCA} are respectively presented figures 5 (bottom left) and (bottom right). If no peculiar velocity field is present (i.e. pure Hubble flow hypothesis, as it is the case for simulated samples), we see that a^{NCA} and B_*^{NCA} estimators are not biased, as it was previously proven appendices B and C (averaged over 1000 simulations, their values coincide with the input slope and "zero-point" of the simulated sample). It illustrates one of the potentialities of the null-correlation approach for calibrating TF like relations, i.e. its insensitivity to observational selection effects in apparent magnitude m and log line-width distance indicator p . For these simulated samples supposed to mimic the Mathewson field galaxies sample ($N_{\text{gal}} = 1127$), accuracy σ_a of the NCA slope estimator a^{NCA} sounds clearly good : $\sigma_a = 0.07$ or 1% of a^D if all the sample is selected, $\sigma_a = 0.1$ if half of the nearby galaxies of the sample are discarded (i.e. $R(r^*) = 0.5$ or $r^* \approx 3000 \text{ km s}^{-1}$) and $\sigma_a = 0.15$ at $r^* \approx 4000 \text{ km s}^{-1}$ (i.e. $R(r^*) = 0.25$)⁵. The same remark holds for the NCA "zero-point" B_*^{NCA} accuracy σ_{B^*} , $\sigma_{B^*} = 0.0003$ or 3% of B^* at $r^* = 0$ and $\sigma_{B^*} = 0.001$ at $r^* \approx 4000 \text{ km s}^{-1}$.

Influence of peculiar velocity field on the NCA estimators is analysed using three examples : "Great Attractor" (GA) flow, constant or bulk flow and gaussian random or Maxwellian flow. In order to take into account the peculiarity of the 3D spatial distribution of the Mathewson field galaxies sample, biases created by these flows have been calculated by comparing the estimates of a^{NCA} , B_*^{NCA} and $\rho(p, \tilde{v})$ when one of these velocity field is added to the observed redshifts of the MAT sample, with these estimates for the real MAT sample. The Maxwellian flow has a velocity agitation of $\sigma_v = 500 \text{ km s}^{-1}$ and the bulk flow has been chosen to point toward direction $l = 310$ and $b = 20$ in galactic coordinates with an amplitude of

⁵ The standard deviation σ_a is proportional to $R(r^*)^{-1/2}$, as expected.

500 km s^{-1} . The GA flow⁶ is the one of Bertschinger et al. 1988, centered at a distance of 4200 km s^{-1} toward $l = 310$ and $b = 20$ and creating an infall velocity for our Local group of 535 km s^{-1} .

Figure 5 (bottom left) illustrates particularly well the discussion of section 3.1 which was based on analytical results. Biases on the NCA slope estimate a^{NCA} created by the presence of Maxwellian and Bulk flows become negligible when nearby galaxies of the MAT sample are discarded using the subsampling procedure in distance estimate (say herein for $r^* > 3000 \text{ km s}^{-1}$). Influence of GA flow can be controled likewise. In practice, large values of the cut-off in distance estimate r^* have to be preferred, of course with regards to the accuracy and to the r^* -dependent statistical fluctuations affecting the NCA slope estimate at this distance r^* .

Influences of velocity fields on B_*^{NCA} and $\rho(p, \tilde{v})$ are shown respectively figures 5 (bottom right) and (top right). As expected, Maxwellian flow does not bias these two quantities. Since the calibration of the simulated samples was not performed line-of-sight by line-of-sight, presence of Bulk flow slightly biases B_*^{NCA} and $\rho(p, \tilde{v})$. On the other hand, we can see that GA flow creates a significative bias on the two quantities (i.e. greater than their standard deviations). The fact that these biases vanish for large values of the cut-off in distance estimate r^* is due to the specific form of the GA flow and to the characteristics of the 3D spatial distribution of the MAT sample. It cannot be interpreted as a general feature since the correlation between p and \tilde{v} is not expected to vanish when the subsampling in distance estimate is applied, as it is the case for the p - $X(a^D)$ correlation. Some reasons may however be advocated for favouring large values of the cut-off in distance estimate r^* . Since such a subsampling selects preferentially far away galaxies, a slighter coherence of their peculiar velocities is expected, consequently to their mutual distances. Finally, one remarks that amplitude of the bias created by huge flows such as the "Great Attractor" is not greater than $\Delta B^* \approx 0.001$, or 10% of the value of B^* . Same remark for the bias on the correlation coefficient $\rho(p, \tilde{v})$ which is less than $\Delta \rho = 0.1$ whatever the value of the cut-off in distance estimate r^* .

D.2. Testing on Mathewson et al. calibration parameters

Mathewson et al. 1992 have proposed some values for the DTF calibration parameters. The authors calibrate the DTF slope a^D in the Fornax cluster (14 galaxies). An estimate of $a^{\text{MAT}} = -7.96$ is obtained by performing a linear regression in magnitude. Assuming that the true distance in km s^{-1} units of Fornax cluster is 1340 km s^{-1} , authors

⁶ Since the real distance of MAT galaxies are not known, the contribution of the radial peculiar velocity inferred by GA flow model to observed redshift has been added under the approximation that galaxies distances are given by their observed redshifts.

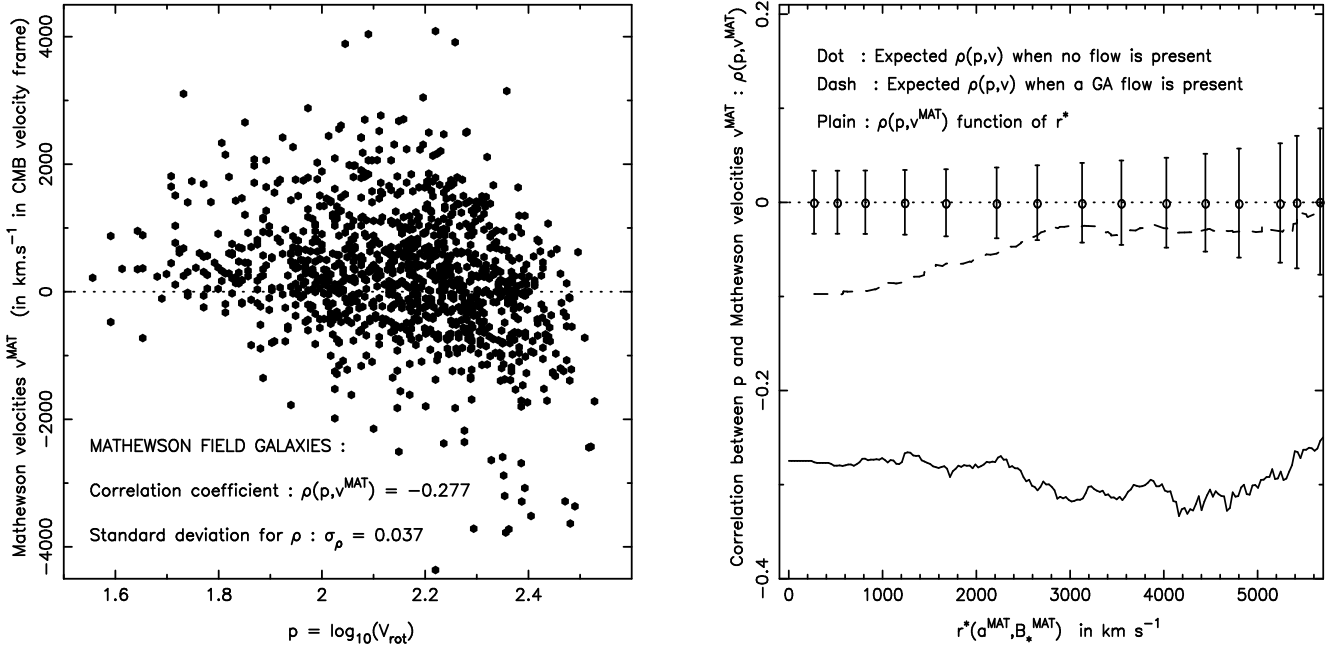


Fig. 6. Correlation between p and Mathewson velocity estimates \tilde{v}^{MAT} .

derived a value of $B^{\text{MAT}} = 0.0039$ for DTF relative zero-point B . If $H_0 = 85 \text{ km s}^{-1} \text{ Mpc}^{-1}$, it implies a value of $b^{\text{MAT}} = -3.31$ for the DTF zero-point b^D . Averaging over the seven richest clusters of their catalog, a value of $\sigma_\zeta^{\text{MAT}} = 0.32$ is estimated for the intrinsic scatter of the DTF relation, which gives a value of $B_*^{\text{MAT}} = 0.0042$ for the DTF relative "zero-point" B^* . No error bars are proposed for these estimates.

Mathewson et al. DTF calibration parameters are tested on figure 6. Figure 6 (left) shows the correlation between p and Mathewson et al. peculiar velocity estimate \tilde{v}^{MAT} for the $N_{\text{gal}} = 1127$ of the MAT sample. Figure 6 (right) shows variations of $\rho(p, \tilde{v}^{\text{MAT}})$ with respect to the cut-off in distance estimate r^* and the deviations from 0 expected when a flow such as the "Great Attractor" is present. It looks very unlikely that the strong correlation found between p and \tilde{v}^{MAT} can be explained by the presence of large scale coherent peculiar velocity field. The same feature is observed for the p - $X(a^{\text{MAT}})$ correlation (not shown). This test leads to question in the validity of the calibration techniques used by Mathewson et al. when deriving slope and relative zero-point of the DTF relation.

As a matter of fact, it is known that the estimator of the DTF slope a^D , obtained in a cluster by a linear regression on m , is biased by the presence of observational selection effects on m and p (see Lynden-Bell et al. 1988 for example). This bias can be corrected on in theory but a full description of selection effects in observation is thus required (see for example Willick 1994), and so is difficult

to realize in practice. Same kind of remark holds for the relative zero-point estimate B . Since existing peculiar velocity field models proposed in the literature are far to be perfect nor accurate, a room of uncertainty remains when attributing a true distance to the calibration cluster (an error of 250 km s^{-1} for the assumed true distance of Fornax cluster will imply a relative error of $\frac{\delta B}{B} \approx 20\%$ for the relative zero-point B).

D.3. NCA calibration of the Mathewson spiral field galaxies sample

NCA calibration is herein performed by following the discussions of section D.1. The NCA estimate of the DTF slope a^D is obtained from a subsample selected in distance estimate beyond 4000 km s^{-1} , which corresponds to discard about 60% of nearby galaxies of the MAT sample. NCA estimate of the DTF "zero-point" B^* was achieved using galaxies beyond 5000 km s^{-1} . Figure 7 shows the results of the NCA calibration of the Mathewson field galaxies catalog⁷.

The value of NCA estimate of the DTF slope a^D is given figure 7 (bottom left) : $a^{\text{NCA}} = -7$. with an accuracy at $r^* = 4000 \text{ km s}^{-1}$ given by the numerical simulations of $\sigma_a = 0.15$ (or in other words $a^{\text{NCA}} = -7 \pm 0.15$). Since

⁷ Since the subsampling procedure in distance estimate depends on the values of a^{NCA} and B_*^{NCA} , few iterations were performed in order to achieve the stable situation presented figure 7.

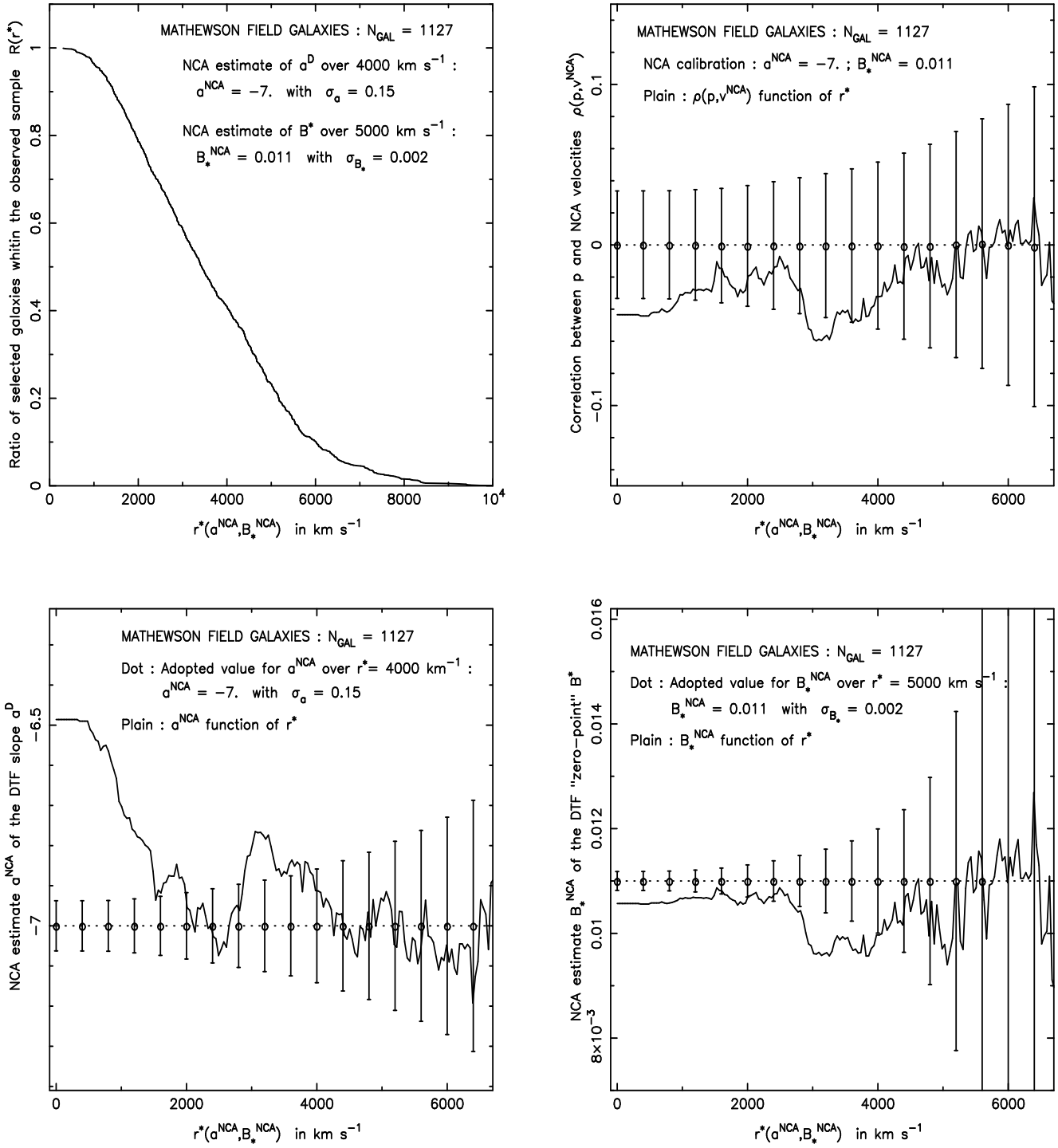


Fig. 7. NCA calibration of the Mathewson spiral field galaxies sample : (Top left) Ratio $R(r^*)$ of selected galaxies within the MAT sample function of the extra cut-off in distance estimate $r^*(a_{\text{NCA}}, B_*^{\text{NCA}})$. (Top right) Correlation coefficient $\rho(p, \tilde{v}^{\text{NCA}})$ between p and NCA peculiar velocity estimate \tilde{v}^{NCA} . (Bottom left) NCA slope estimate a^D function of the extra cut-off in distance estimate $r^*(a_{\text{NCA}}, B_*^{\text{NCA}})$. (Bottom right) NCA relative "zero-point" estimate B^* function of the extra cut-off in distance estimate $r^*(a_{\text{NCA}}, B_*^{\text{NCA}})$.

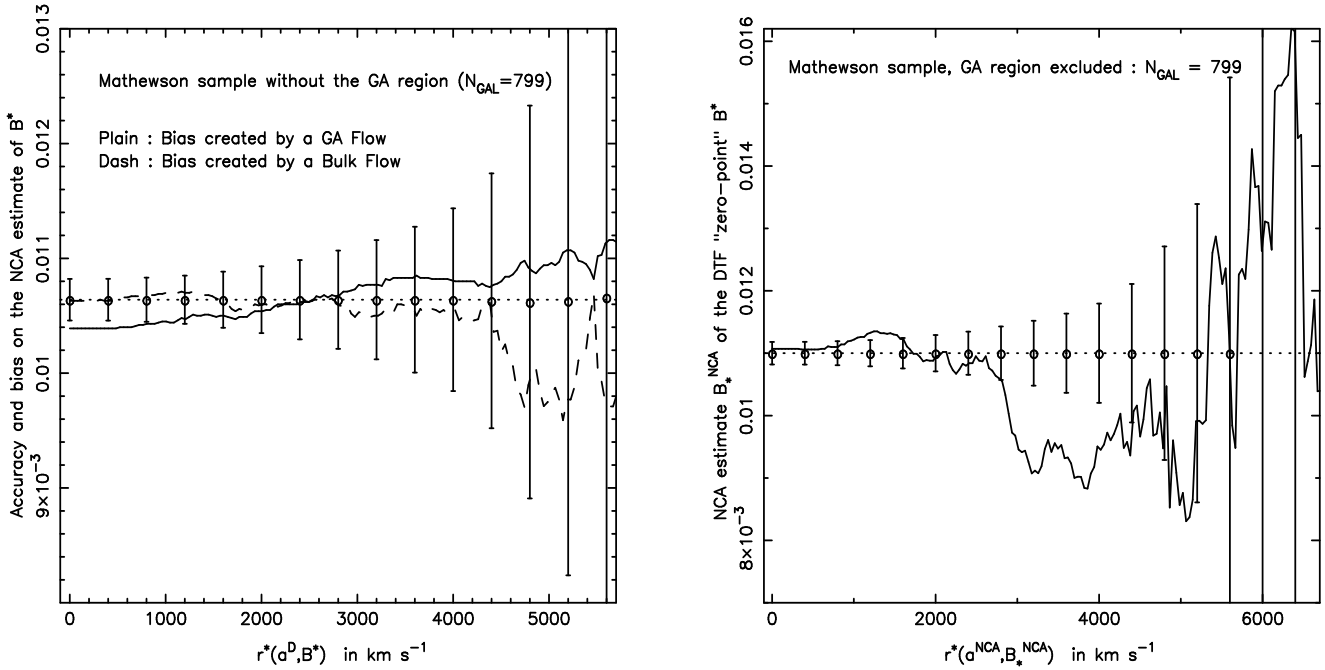


Fig. 8. NCA "zero-point" estimate for $N_{\text{gal}} = 799$ remaining galaxies of the MAT sample when excluding the GA region (defined as a conic area pointing toward $l = 310$ and $b = 20$ with an angular aperture of 45°) : (Left) Standard deviation for NCA "zero-point" estimator B_*^{NCA} and velocity biases created by GA and Bulk flows. (Right) NCA "zero-point" estimate B_*^{NCA} function of the extra cut-off in distance estimate $r^*(a^{\text{NCA}}, B_*^{\text{NCA}})$.

this estimate is obtained with a large cut-off in distance estimate, it is in principle free of biases created by large scale peculiar velocity field. Adding to this point that NCA calibration technique is insensitive to observational selection effects on apparent magnitude m and log line-width distance indicator p , NCA estimate of DTF slope a^D appears as fairly secure.

NCA estimate of the relative "zero-point" B^* is shown figure 7 (bottom right). The value of $B_*^{\text{NCA}} = 0.011$ has been arrested accounting for the more or less stable trend of B_*^{NCA} beyond $r^* = 5000 \text{ km s}^{-1}$. To give a value of the B_*^{NCA} accuracy is a little bit more tricky. It was previously mentioned that the subsampling procedure in distance estimate does not remove bias on B_*^{NCA} estimator created by the presence of large scale peculiar velocity field (excepting the case of bulk flows). It turns out that the value of this bias depends on the specific geometry and amplitude of the real cosmic velocity field, and so cannot be estimated without modeling this velocity field. The amplitude of this bias for the "Great Attractor" flow model is less than $\Delta B = 0.001$ (or about 10% of B^*) for the MAT sample. It means that if the GA flow is real, error on B_*^{NCA} estimator is dominated by velocity bias rather than statistical fluctuations (accounting for the value of the accuracy on B_*^{NCA} obtained from numerical simulations). At this stage, other criterion for calibrating DTF

relative "zero-point" B^* may be preferred, for example in constraining the average $\langle \tilde{v} \rangle$ of radial peculiar velocity estimates over the sample to vanish. Unfortunately such property $\langle \tilde{v} \rangle = 0$ is theoretically expected for fair samples (i.e. samples large enough to be representative at any scales of the kinematical fluctuations of the Universe), but not expected for catalogs such as the MAT sample.

Amplitude of velocity bias on the B_*^{NCA} estimator may however be attenuated by removing of the sample areas presumed to have a strong kinematical activity. Such a procedure was achieved by discarding galaxies of the MAT sample belonging to a cone pointing toward $l = 310$ and $b = 20$ in galactic coordinates with an angular aperture of 45° (the GA region). This subsample (i.e. MAT sample, GA region excluded) contains $N_{\text{gal}} = 799$ galaxies. Figure 8 (left) shows amplitudes of biases created by bulk and GA flow when the GA region is excluded of the MAT sample. Compared to the biases shown figure 5 (bottom left) for the whole MAT sample, the discarding procedure looks efficient (if of course, the "Great Attractor" model of Bertschinger et al. 1988 succeeds in mimicking the real cosmic peculiar velocity field). Figure 8 (right) shows the NCA estimate B_*^{NCA} for the MAT sample, GA region excluded. If the situation improves for $r^* < 3000 \text{ km s}^{-1}$ (compared to figure 6 (bottom left) showing B_*^{NCA} for the whole MAT sample), a residual bias persists between

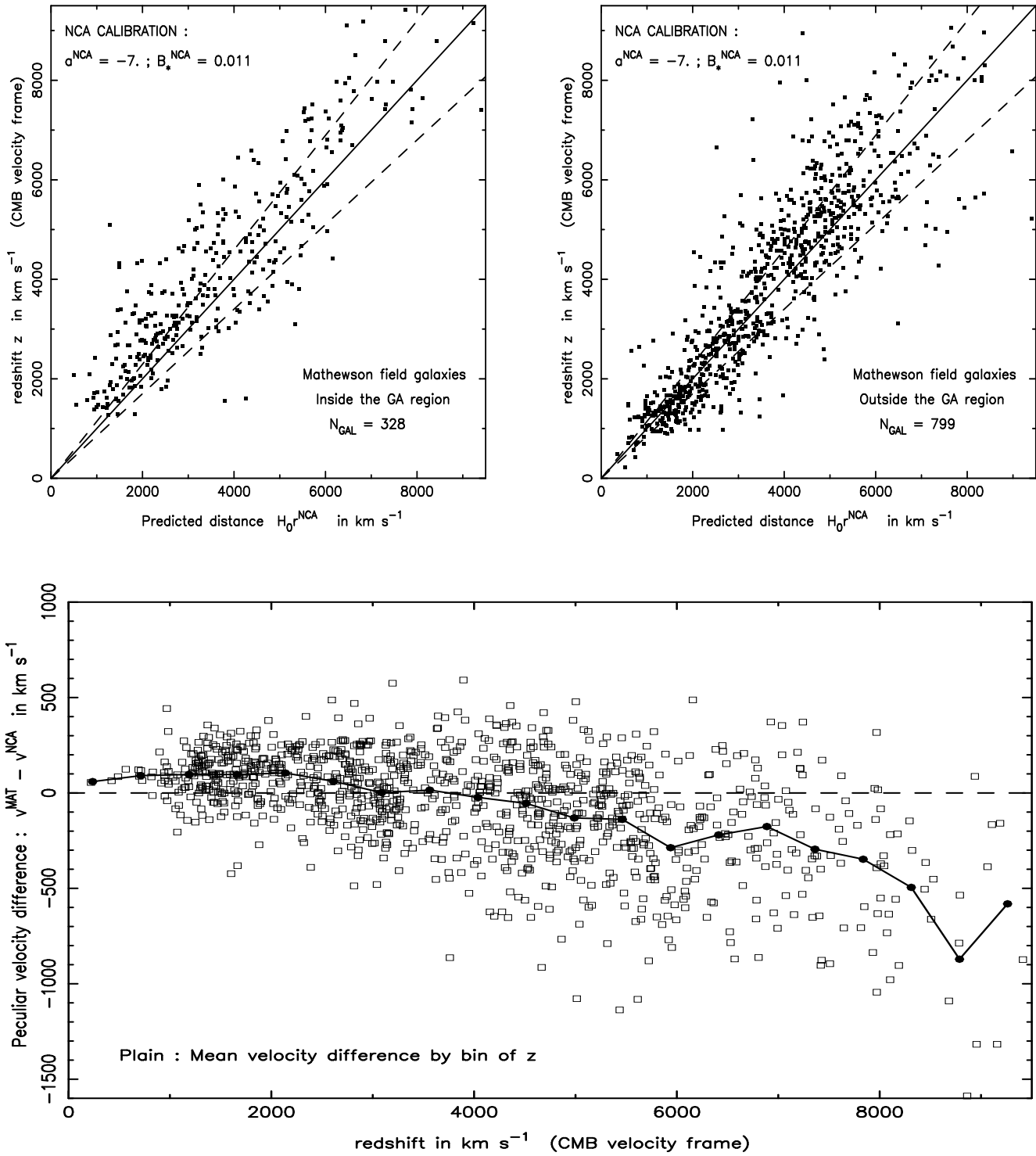


Fig. 9. Top : Redshifts z versus NCA distance estimates in km s $^{-1}$ for the MAT sample (left) Outside the GA region (right) Inside the GA region. Bottom : Peculiar velocity difference between Mathewson velocity estimates \tilde{v}^{MAT} and NCA velocity estimates \tilde{v}^{NCA} .

$r^* = 3000 \text{ km s}^{-1}$ and $r^* = 5000 \text{ km s}^{-1}$. The value of the NCA relative "zero-point" $B_*^{\text{NCA}} = 0.011$ has then to be read cautiously, keeping in mind that it can be affected by a velocity bias (anyway presumed not to be greater than $\Delta B = 0.001$)⁸.

Finally, distance estimate \tilde{r} and velocity estimate \tilde{v} given respectively Eq. (6) and Eq. (20) can be inferred using the NCA calibration parameters $a^{\text{NCA}} = -7$. and $B_*^{\text{NCA}} = 0.011$ previously derived. Figure 9 (left) and (right) show respectively the redshift z versus the NCA predicted distance $H_0 \tilde{r}^{\text{NCA}} = B_*^{\text{NCA}} \exp[\alpha(m - a^{\text{NCA}} p)]$ for galaxies of the MAT sample outside and inside the GA region. Figure 9 (bottom) illustrates the difference between the peculiar velocity estimates $\tilde{v} = z - B_* \exp[\alpha(m - a^D p)]$ of Mathewson et al. 1992 and the ones derived in this present appendix. The averaged velocity difference by bins of redshift z is plotted function of the redshift. It turns out that an erroneous input value of the calibration parameters can interpret, especially at large redshifts, as fictitious large scale and coherent peculiar velocity flows. The preliminar calibration step of Tully-Fisher like relation is thus of crucial importance for kinematical studies.

References

Aaronson M., Bothun G., Mould J., Huchra J., Schommer R. A. and Cornell M. E., 1986, *ApJ* 258, 64

Bertschinger E. and Juszkiewicz R., 1988, *ApJ Letters* 334, L59

Bertschinger E., Dekel A., Faber S. M. and Burstein D., 1990, *ApJ* 364, 370

Bicknell G. V. 1992, *ApJ* 399, 1

Bottinelli L., Gouguenheim L., Paturel G. and Teerikorpi P. 1986, *A&A* 156, 157

Dekel A., 1994, *Ann. Rev. A&A* 32, 371

Ekholm T. 1996, *A&A* 308, 7

Faber S. M. and Jackson R., 1976, *ApJ* 204, 668

Fouqué P., Bottinelli L., Gouguenheim L. and Paturel G. 1990, *ApJ* 349, 1

Hendry M. A. and Simmons J. F. L. 1990, *A&A* 237, 275

Hendry M. A. and Simmons J. F. L. 1994, *ApJ* 435, 515

Hendry M. A., Rauzy S., Salucci P. and Persic M., 1996, *Astrophys. Letters&Comm.* in press (astro-ph/9508138)

Landy S. D. and Szalay A. 1992, *ApJ* 391, 494

Lynden-Bell D., Dressler A., Burstein D., Davies R. L., Faber S. M., Terlevich R. J. and Wegner G., 1988, *ApJ* 326, 19

Mathewson D. S., Ford V. L. and Buchhorn M., 1992, *ApJ Supp. Series* 81, 413

Newsam A. M., Simmons J. F. L. and Hendry M. A., 1995, *A&A* 294, 627

Rauzy S., Lachièze-Rey M. and Henriksen R. N., 1992, *A&A* 256, 1

Rauzy S., Lachièze-Rey M. and Henriksen R. N., 1995, *Inverse Problems* 11, 765 (astro-ph/9510017)

Rauzy S. and Triay R., 1996, *A&A* 307, 726

Sandage A. 1994, *ApJ* 430, 13

Schechter P.L. 1980, *Astron. J.* 85, 801

Teerikorpi P., 1990, *A&A* 234, 1

Triay R., Lachièze-Rey M. and Rauzy S., 1994, *A&A* 289, 19

Triay R., Rauzy S. and Lachièze-Rey M. 1996, *A&A* 309, 1

Tully R. B. and Fisher J. R., 1977, *A&A* 54, 661

Willick J. A. 1994, *ApJ Supp. Series* 92, 1

Willick J. A., Courteau S., Faber S. M., Burstein D. and Dekel A., 1995, *ApJ* 446, 12

Willick J. A., Courteau S., Faber S. M., Burstein D., Dekel A. and Kolatt T., 1996, *ApJ* 457, 460

⁸ Independently to these velocity bias problems, relative "zero-point" estimator always suffer from an additional bias inherited from the statistical uncertainties on the slope estimate (i.e. $\delta B/B \approx \alpha < p > \delta a^D$)